CHALMERS
UNIVERSITY OF TECHNOLOGY

Modelling the effects of railway-implemented low-height noise screens

An investigation of train track ballast impedance

Master's Thesis in Applied Acoustics

MARIUS HILDÉN

DEPARTMENT OF ARCHITECTURE AND CIVIL ENGINEERING
DIVISION OF APPLIED ACOUSTICS

CHALMERS UNIVERSITY OF TECHNOLOGY
Gothenburg, Sweden 2024
www.chalmers.se

MASTERS'S THESIS 2024

Modelling the effects of railway-implemented low-height noise screens

An investigation of train track ballast impedance

MARIUS HILDÉN

CHALMERS
UNIVERSITY OF TECHNOLOGY

Department of Architecture and Civil Engineering
Division of Applied Acoustics
CHALMERS UNIVERSITY OF TECHNOLOGY
Gothenburg, Sweden 2024

Modelling the effects of railway-implemented low-height noise screens
An investigation of train track ballast impedance
MARIUS HILDÉN

Supervisor: Magnus Källman, Trafikverket / Swedish Transport Administration
Examiner: Jens Forssén, Division of Applied Acoustics

Master's Thesis 2024

Department of Architecture and Civil Engineering
Division of Applied Acoustics
Chalmers University of Technology
SE-412 96 Gothenburg
Telephone +46 31 772 1000

Typeset in LaTeX
Gothenburg, Sweden 2024

Abstract

Conventional tall noise barriers (measuring approximately 3 meters and above) are commonly employed to mitigate noise from railways in urban environments. They are effective and their noise reduction outcomes can be accurately estimated using existing, low-order geometrical ray-acoustic models, e.g. Pierce's thin hard diffracting screen solution.

However, tall noise barriers arguably have an adverse effect on surrounding landscape, as well as obscuring the sightlines of both train operators and passengers. In cases where noise levels can be adequately attenuated using a low-height noise screen (**LHNS**) it can be a preferable implementation in regard to aesthetic, cost, and maintenance aspects.

The current problem with implementing LHNS is that their noise reduction outcomes are, due to fundamental design, difficult to accurately estimate. This is a problem in large-scale urban development projects where the margin of error is small, often leading to LHNS being disregarded in favor of conventional noise screens.

To improve the accuracy of insertion loss (**IL**) estimations from LHNS, a previously implemented 2.5D boundary element method (**BEM**) model used for calculating railway LHNS IL is revised. The main focus of the revision regards the surface impedance of the BEM-modeled train track.

Measurements have been performed on ballasted train tracks to serve as validation data for an impedance parameter study of ballasted train track surfaces. The resulting set of impedance parameters have been used in 2.5D BEM-models simulating the sound pressure field of different train shapes with and without LHNS, in other words estimating the IL of LHNS for different railway applications. The IL results are compared with existing LHNS IL measurements from other projects.

The simulated results demonstrate a generally accurate alignment with existing measurement data for IL in third-octave frequency bands for passenger trains, however results differ between different measurement comparisons. In the case of industrial trains, results are less promising. This is hypothesized to be a result of the source model used in the simulations being inaccurate for industrial trains.

Further investigation/development of source models used for different train types is a recommended starting point for improving the reliability of the 2.5D BEM simulations. Access to more LHNS IL measurement validation data is also considered necessary. Nonetheless, the yielded results indicate that the revised impedance parameters have been an effective step in improving LHNS IL estimation when compared with previous BEM-model results.

Keywords: low-height noise screen, low-height noise barrier, ballast impedance, acoustics, insertion loss, BEM.

Acknowledgements

I would like to express my sincere gratitude to my supervisor Magnus Källman as well my examiner Jens Forssén. Their guidance, support and constructive feedback throughout the thesis process has been invaluable. I am also grateful to Monica Waaranperä and Jonas Rajalin for their help in defining the contents of the thesis.

Finally I want to extend a special thank you to everyone at the Division of Applied Acoustics, who have been a source of inspiration and motivation since day one of the master's programme.

Marius Hildén
Gothenburg, February 2024

Contents

1
Introduction

1.1 Background

Traditional tall noise screens (3 m and above) are a widely used noise reduction measure in urban settings. They are effective and, most importantly, predictable in terms of resulting noise reduction. The insertion loss (**IL**) of such screens can be calculated accurately using existing calculation models. However, there are cases where a noise reduction measure is necessary, but tall noise screens can be deemed excessive. In these cases, low-height noise screens (**LHNS**) could potentially be utilized instead. Generally, LHNS are less resource costly, easier to maintain, and are less environmentally intrusive. However, a current obstacle preventing widespread implementation of LHNS is accurately estimating resulting IL.

The Swedish Transport Administration (**STA**) is interested in expanding the possible use cases of LHNS, particularly in the case of railway applications. As a step in furthering this goal, the STA has proposed an investigation on improving the modelling possibilities of noise reduction from LHNS.

The underlying problem is that no sufficiently viable calculation models for LHNS exist to use in the planning stage of projects at the scale that the STA conduct. Currently, according to the STA, if train tracks are planned to be placed near an urban area, the implemented noise reduction measure tends to be a traditional tall noise screen. This is the case even if there is reason to believe that a low height noise screen is sufficient.

This Master's thesis is a direct continuation of the work made in P. Eriksson's "Investigation of Prediction Methods for Low Height Noise Barrier Implementation" [1], in which a 2.5D Boundary Element Method (**BEM**) model initially developed by B. Van Der Aa [2] was revised to enable implementation for calculating IL in railway settings. In the report by P. Eriksson, 2 key recommendations are made regarding improvements of the calculation model; the first being an investigation into the different sub-sources of specific train types. The second recommendation regards improving the implemented impedance model. This report will focus on improving the impedance model used in the BEM-simulations.

In the BEM-model used in [1], only one set of finite impedance parameters could be applied to geometries created in the model. Meaning that all finite impedance surfaces in the model would be considered acoustically identical. In the current iteration of the BEM-model, multiple different impedance models can be used on different surfaces.

1.2 Aim

The primary objective of this thesis is to improve the 2.5D BEM model that was implemented in Patrik Eriksson's previous thesis. The ultimate goal is to create a calculation model that is suitably robust and applicable for implementation in STA projects.

1.3 Scope

Due to sharing the same thesis goal and approximately the same BEM model as found in [1] a lot of information that is relevant to the thesis at hand is also described in [1]. As such, detailed information regarding the BEM-implementation will be summarized. Interested readers are encouraged to read P. Eriksson's thesis.

The calculation model will primarily focus on Swedish train tracks and the regulations and standards in place there. The model potentially can be adjusted to be valid for other regions.

The upper frequency limit of calculated BEM results will be 3150 Hz due to an exponential relation between frequency and computational load.

The focus of the report will be in improving the impedance-parameters used in the modelled train track-surface.

1.4 Structure

The report is structured in a way as to answer the central questions of the thesis:

- Will tuning the impedance model used in the BEM-model improve results?
- How can the BEM-model be improved upon further?

In order to present an answer to these questions, the thesis will be divided into three primary chapters (Chapter 2 - Chapter 4). Chapter 2 compiles and presents information considered valuable for understanding how the BEM-model functions. Chapter 3 describes the method used to build upon the existing BEM-model, as well as detailing how the numerical results from the BEM model can be compared with real-world measurements. In chapter 4 the results from current and previous iterations of the BEM-model are compared and discussed. Based on obtained results, eventual shortcomings in the BEM-model are also discussed, as well as recommended improvements for future work.

2

Theory

This chapter aims to provide the reader with a general understanding of the relevant topics discussed and utilized in the thesis.

2.1 Modelling sound propagation

In order to provide context for the implementation of the BEM model, a brief overview of relevant sound propagation factors will be summarized.

Impedance

One of the central concepts to grasp within the context of this thesis is the effect that changes in impedance have on reflected and transmitted sound waves. Impedance, often denoted $\underline{Z}$, is defined as the ratio between two interdependent quantities, such as force and velocity. In the case of sound propagation this ratio is generally between sound pressure and velocity. Impedance is generally a complex quantity, containing both a real and imaginary part. In acoustical terms the impedance of a medium contains both magnitude and phase information. [3]

There are 3 similar but distinct definitions of impedance that are important to keep in mind for the context of this report. These are:

- *Characteristic impedance*, generally denoted $\underline{Z}_0$
- *Specific acoustical impedance*, generally denoted $\underline{Z}_S$
- *Acoustical impedance*, generally denoted $\underline{Z}_A$

Characteristic impedance, $\underline{Z}_0$, is the most fundamental definition of the three, it describes the ratio of sound pressure and particle velocity in the context of an infinite plane wave. Assuming that there are no propagation losses in the medium this impedance type is generally a real value, containing no imaginary component. In these cases $\underline{Z}_0 = Z_0 = \rho_0 c_0$, where ρ_0 and c_0 denotes the density and speed of sound the medium respectively. The unit of characteristic impedance is $\frac{Ns}{m^3}$, known as Rayl. This type of impedance is sometimes called characteristic impedance due to it characterizing the medium itself.

Specific acoustical impedance, $\underline{Z}_S$, shares the same unit as characteristic impedance, $\frac{Ns}{m^3}$, and is similar in its definition. The difference between the two is that sound field impedance contains a directional aspect. Sound field impedance is defined as the ratio of sound pressure to particle velocity in the reference direction at a specific point in the medium. Some literature refers to this quantity with the term *sound field impedance*.

Acoustical impedance, $\underline{Z}_A$, is in turn similar to sound field impedance. The difference between the two in this case is that acoustical impedance describes the ratio of sound pressure to volume velocity in the normal direction to a specific reference surface in an acoustic system. Volume velocity can be denoted U and is the product of the normal direction of particle velocity and a surface area of interest. The particle velocity and phase is simplified as being constant in magnitude and phase over the surface of consideration. In this sense volume velocity essentially describes the volume of particles that passes in the normal direction of a specific surface area.

Reflection / transmission at impedance boundaries

If a sound wave approaches a boundary in which the characteristic impedance changes, e.g. on the boundary between two mediums, the result will generally be that the sound wave splits. One part of the incident sound wave will be transmitted into the new impedance region while another part will be reflected. An illustration of this phenomena can be found in figure 2.1, where a plane wave in one medium with characteristic impedance $\underline{Z}_{0,1}$ ('phase 1') is incident on another medium with the characteristic impedance $\underline{Z}_{0,2}$ ('phase 2') at an angle of θ_i relative to the normal of the boundary between the two mediums. The collision results in a reflected wave at an angle of θ_r in the same medium as the incident wave and a transmitted wave at an angle of θ_t in the secondary medium.

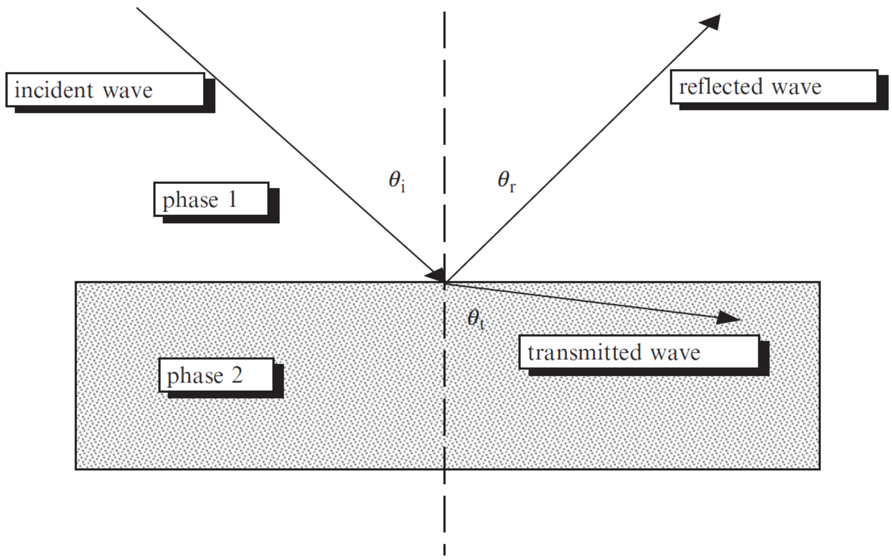

Figure 2.1: *Sound propagation at a boundary between two media [4].*

The relation between the incident wave and the reflected/transmitted waves are determined by the characteristic impedances $\underline{Z}_{0,1}$ and $\underline{Z}_{0,2}$ in each medium as well as the angles θ_i and θ_t. The ratio between the reflected and transmitted plane wave can be described with a complex reflection factor $\underline{r}$ with the following expression.

$$\underline{r} = \frac{\underline{Z}_{0,2}\cos(\theta_i) - \underline{Z}_{0,1}\cos(\theta_t)}{\underline{Z}_{0,2}\cos(\theta_i) + \underline{Z}_{0,1}\cos(\theta_t)} \tag{2.1}$$

In the case of outdoor sound propagation, i.e. medium 1 consisting of air and medium 2 generally consisting of a more or less rigid surface, it can be assumed that medium 2 is a locally reacting surface, meaning that the transmitted wave propagates at an angle normal to the surface ($cos(\theta_t)$). In this case the equation above can be rewritten as:

$$\underline{r} = \frac{\frac{\underline{Z}_{0,2}}{\rho_0 c_0}\cos(\theta_i) - 1}{\frac{\underline{Z}_{0,2}}{\rho_0 c_0}\cos(\theta_i) + 1} \tag{2.2}$$

Where ρ_0 is air density, c_0 is the speed of sound in air and the term $\frac{\underline{Z}_{0,2}}{\rho_0 c_0}$ is the impedance of medium 2 normalized to air. In other words the term describes the second mediums normalized impedance. From the equation it can be seen that as $\underline{Z}_{0,2} \to \infty$, $\underline{r} \to 1$, meaning total reflection. When $\underline{Z}_{0,2} \to 0$ and/or $cos(\theta_i) \to 0$ however it can be deduced that $\underline{r} \to -1$, meaning sound is reflected with an inverted phase, potentially leading to a sound pressure reduction due to destructive interference.

In the case of outdoor sound propagation the assumption of plane wave propagation is however insufficient. This is the case because sound must be modelled as propagating spherically when the incident angle θ_i and/or wavelength is high. The curvature of the wavefront has an impact on the reflected sound. This is accounted for by adapting the plane wave reflection factor $\underline{r}$ to a spherical reflection factor, denoted $\underline{Q}$, and is expressed as following [5] :

$$\underline{Q} = \underline{r} + (1 - \underline{r})BG(\omega) \tag{2.3}$$

where $BG(\omega)$ is a factor that adjusts the plane wave reflection factor to be applicable for spherical waves. Because this factor is not essential to understand the core concept it will not be given further explanation in this section, but one is available in [5].

Scattering and diffraction

Placing a barrier that obstructs the direct path of a sound wave between a sound source and receiver position impacts the path of sound waves between source and receiver. Such an obstruction causes part of the sound to be reflected away from the receiver, as well as diffracting the sound waves in the path to the receiver, resulting in a reduction in sound pressure level. If the receiver position is obstructed from the direct path of sound from the source, the reciever is in the so called *shadow zone*.

A simplified illustrative example of this phenomenon can be seen in figure 2.2, where a sound source places at height h_S relative to ground plane is radiating sound waves to a receiver placed at height h_R. The direct sound is however obstructed by a barrier with height h_B, meaning that the receiver in this case is in the shadow zone.

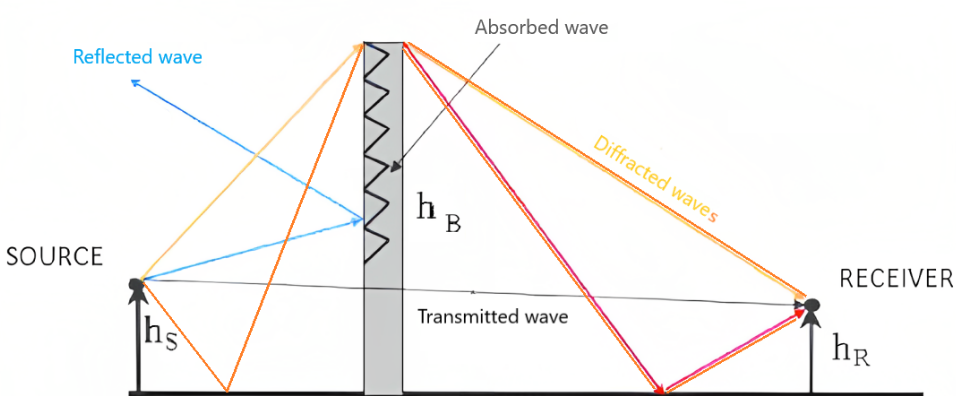

Figure 2.2: *Simplified representation of different wave paths in the presence of barrier [6].*

As can be interpreted from the figure, the sound can be simplified as propagating to the receiver in 5 different paths that can be summarized as the following:

- $\underline{p}_1$, The purely diffracted wave with no reflections on source or reciever side seen in the *yellow* line
- $\underline{p}_2$, the source side-only reflected wave seen in the top *orange* line.
- $\underline{p}_3$ the receiver side-only relected wave seen in the *red* line.
- $\underline{p}_4$ the source & receiver side reflected wave seen in the bottom *orange* line.
- $\underline{p}_5$ The wave transmitted through the barrier, seen in the thin *black* line.

In the context of a rigid barrier in outdoor environments, the influence from the transmitted wave $\underline{p}_5$ on the resulting sound pressure in the receiver is negligible, and will therefore be omitted from this point on.

This makes the resulting sound pressure in the receiver a sum of the different propagation paths multiplied by the spherical reflection coefficient(s) of the reflecting surface(s) which can be expressed as follows:

$$\underline{p}_{tot} = \underline{p}_1 + \underline{Q}_S \underline{p}_2 + \underline{Q}_R \underline{p}_3 + \underline{Q}_S \underline{Q}_R \underline{p}_4 \tag{2.4}$$

Where $\underline{Q}_S$ and $\underline{Q}_R$ represent the spherical reflection factors of the source-side and receiver-side ground respectively. In other words the resulting sound pressure level at the receiver position is influenced by the reflection factor, and in extension, the normalized impedance of the reflecting surfaces.

2.1.1 Impedance modeling

In order to accurately estimate the characteristic impedance Z_0 and complex wave number $\underline{k}$ of a material, some sort of impedance model is necessary to utilize. Impedance models deemed relevant for the purposes of this report will be summarized in this section.

Delaney and Bazley

The Delaney and Bazley model of impedance, sometimes referred to as the one parameter-model, is based on a significant number of measurements on fibrous materials presented in the report *ACOUSTICAL PROPERTIES OF FIBROUS ABSORBENT MATERIALS* [7] The model is widely used for its simplicity, using only one input parameter for estimating Z_0 and $\underline{k}$. This parameter is flow resistivity (σ), defined as the airflow resistance through a material.

Identical tortuous pores (Slit-Pore)

The identical tortuous pores model can generally be used for materials with differing degrees of porosity, one such example could be considered ballast.

The model assumes a material with a surface with a thickness d that is assumed to have a determined number of arbitrarily shaped pores, the complexity of which can be decided on a case by case basis. for the purposes of mathematical convenience, as well as relatively negligible impact of pore shape [8], this report will consider a material containing identical tortuous pores in the form of parallel-walled slits. The relevant parameters used for the slit-pore model in this report can be explained as follows:

- d - layer thickness, used for calculating surface impedance. (m)
- σ - flow resistivity
- ϕ - porosity

The slit pore model will be the one used for the train track in the report.

2.2 Modeling noise from railways

This section describes the considerations of note when modeling the sound in connection to railway infrastructure, with a focus on the effect of LHNS.

2.2.1 The design concept of railway-implemented LHNS

LHNS typically incorporate some sort of sound-absorbing material on the side facing the noise source. The use of absorbent materials is impactful due to the large number of reflections occuring between the body of the train and the screen. See figure 2.3 for an illustration of this. The

Typically, a Low-Height Noise Screen (LHNS), in contrast to standard high screens, functions by introducing some type of absorbent material on the side of the barrier that faces the noise source. Since the screen is positioned relatively close to the source, the additional attenuation due to an extended propagation path is not substantial. Instead, the screen depends on the absorption within the barrier, train, and ballast to dissipate energy through numerous reflections, as illustrated in Figure 2.1. This is why most traditional calculation methods based on geometrical ray acoustics struggle to accurately predict the Insertion Loss (IL) of an LHNS. These methods typically rely on diffraction and/or ray tracing of the direct sound and reflections up to approximately the third order.

Attenuation between rail and boogie

Attenuation between train and LHNS

Figure 2.3: *Illustration of reflection patterns caused by LHNS [9].*

2.2.2 Train source modeling

Due to the limited height of an LHNS, the location of sound sources on the train body is a determining factor in accurately estimating IL as a result of these types of screens. The placement, characteristics and number of sound sources on a train varies greatly between different types of trains. In the noise calculation method Nord2000 - Rail source model [10], principle source locations for trains are given as seen in figure 2.4.

	Height above top of rail (m)	Horizontal location
Source 1 Wheel/rail	0,01	Evenly distributed along the train
Source 2 Wheel/rail	0,35 x wheel diameter	Evenly distributed along the train
Source 3 Wheel/rail	0,70 x wheel diameter	Evenly distributed along the train
Source 4 Engine	Actual height	Centre of engine openings.
Source 5 Exhaust	Actual height of exhaust	Exhaust outlet
Source 6 Aerodynamic	To be determined in each case	To be determined in each case

Figure 2.4: *Principle source locations for trains [10].*

In the case where details regarding the train are unknown, the report suggests using the default source characteristics and locations found in figure 2.5.

	Height above top of rail (m)	Frequency range 1) (Hz)	Horizontal location
Source 1 Wheel/rail	0,01	200 - 10000	Evenly distributed along the train
Source 2 Wheel/rail	0,35	200 - 10000	Evenly distributed along the train
Source 3 Wheel/rail	0,70	200 - 10000	Evenly distributed along the train
Source 4 Engine/Exhaust	2,5	25 - 160	Centre of engine openings.

1) Often frequencies below 50 Hz and above 5000 Hz can be neglected.

Figure 2.5: *Default source values for trains [10].*

The Nord2000 report states that the ideal scenario is to know the source strength and characteristics of each sub source in the specific train type in question, but also concludes that not enough data is available to reliably achieve this. For the puroposes of this report, only the wheel/rail subsources will be considered, and they are assumed to be placed at the default locations in figure 2.5.

In addition to knowing the placement of the different sources on the train it is important to know the energy distribution between the different sources. An investigation of this has been done on an X2000 train in the report *Prediction of high-speed train noise on Swedish tracks* [11]. The results from the report are fine-tuned in the report *Tuning of the acoustic source model* [12]. Findings of the sound power emitted from different sources are presented in figure 2.6. The presented results are for the speeds 40 km/h and 70 km/h.

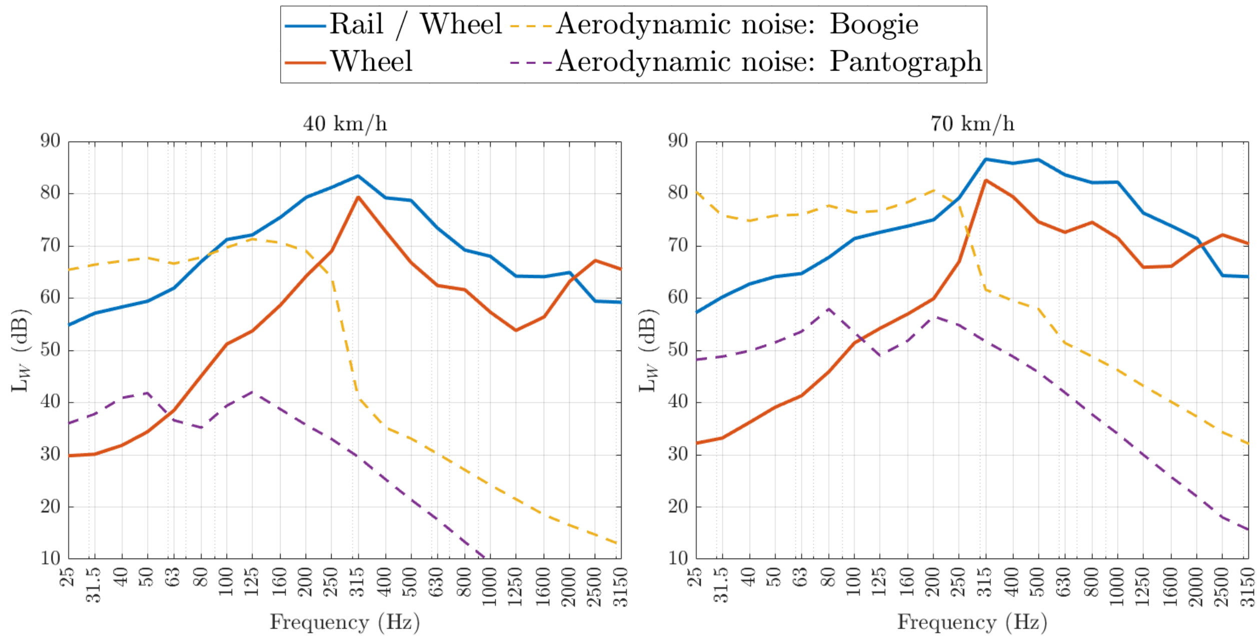

Figure 2.6: *Sound power generated by different sub-sources of a X2000-train [12].*

2.3 Summary of BEM theory and implementation

The following section is a summarized version the information found in chapter 3 of [1]. Readers interested in more detailed explanations surrounding the theory and structure of the BEM-code implementation are encouraged to read [1].

2.3.1 The Kirchhoff-Helmholtz integral

Consider the cross section of a train with train tracks and a LHNS. An illustrative example of this can be found in figure 2.7. In this figure two sets of surface segments, S_{train} & S_{track} are enclosing the volumes V_{train} & V_{track} that exist in V_{free}.

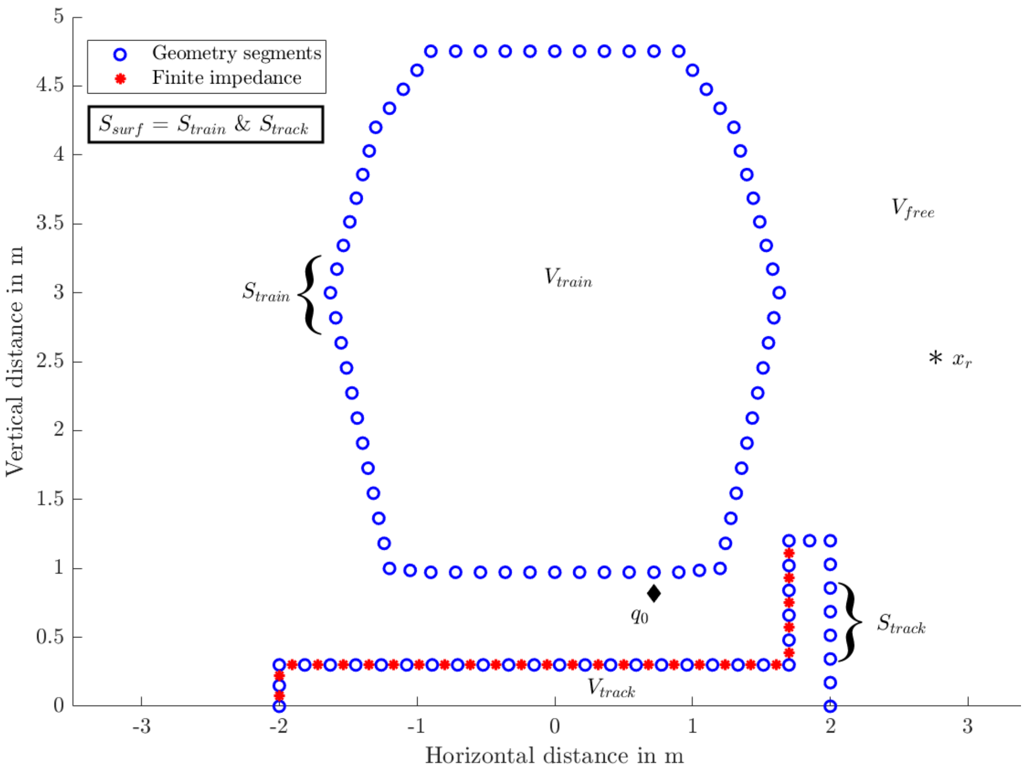

Figure 2.7: *Illustrative example of the concepts discussed in subsequent text.*

For illustrative purposes a source q_0 with a given shape function and reciever x_r have been placed at arbitrary coordinates within V_{free}. Assuming that both the source and receiver positions are placed within V_{free}, The pressure in receiver x_r caused by direct and surface-reflected pressure from source q_0 can be expressed as:

$$\left.\begin{array}{c}\text{If } x_r \in V_{free} \text{ and } \notin S_{surf}, 1 \\ \text{If } x_r \in S_{surf}, \frac{1}{2} \\ \text{else, } 0\end{array}\right\} \cdot p\left(x_r\right) = \underbrace{\frac{1}{4\pi}\int_V \frac{e^{-jkR}}{R} q_0 dV}_{\text{Volume source } = p_{q_0}} \dots$$

$$+ \frac{1}{4\pi}\int_S \frac{e^{-jkR}}{R} p_s(\underbrace{jk\beta}_{\text{Monopole layer}} - \underbrace{\left(jk + \frac{1}{R}\right)(\vec{e}_R \bullet \vec{n}_S)}_{\text{Dipole layer}})dS \tag{2.5}$$

Where V is the area of V_{free}, k is the wave number, R is the distance between source q_0 and receiver x_r, S is the surface of a given area (e.g. S_{train} / S_{track}), p_s is the pressure on S_{surf},

β is the normalized impedance of a given surface, $\vec{e}_R$ is a unit vector of the direction between source and receiver, $\vec{n}_S$ is the unit vector normal to a given surface.

β is in the surfaces with red dots in figure 2.7 defined as an impedance model, as discussed in section 2.1.1, while all other surfaces are defined as having infinite normalized impedance.
By placing the receiver x_r at S_{surf} and solving for pressure, equation 2.5 can be expressed as:

$$\frac{1}{2}p\left(x_r \mid S_{surf}\right) = p_{q0} + \frac{1}{4\pi}\int_S p_s \frac{e^{-jkR}}{R}\left(jk\beta - \left(jk + \frac{1}{R}\right)\left(\vec{e}_R \bullet \vec{n}_S\right)\right)dS \tag{2.6}$$

2.3.2 Numerical approximation of the Kirchhoff-Helmholtz integral

Solving the Kirchhoff-Helmholtz integral analytically is in geometrically complex cases, such as in this case, not feasible due to mathematical complexity. Because of this calculations are left to computers. In order to enable computer-aided solving of the problem it must be converted to the numerical domain. This is done by discretizing the continuous surface S_{surf} into smaller elements $S_N = \{1, 2, 3 \ldots N\}$. In figure 2.7 these elements are represented by blue circles. In the numerical domain equation 2.6 can be rewritten as:

$$\frac{1}{2}p_{s,i}\left(x_r \mid S_N\right) = p_{q0,i} - \sum_{j=1}^{N} p_{s,j}\frac{e^{-jkR_j}}{R_j}\left(jk\beta - \left(jk + \frac{1}{R_j}\right)\left(\vec{e}_{R_j} \bullet \vec{n}_{S_j}\right)\right)\Delta S_j \tag{2.7}$$

Where $p_{s,i}$ is the pressure at surface element S_i, $p_{q0,i}$ is the contributing pressure from the source at S_i and $p_{s,j}$ is the contributing reflected pressure at S_i from surface element S_j. When the surface pressure of all elements ($p_{s,N}$) have been determined, the total pressure at any receiver position x_r within V_{free} can be expressed as the sum of pressures from source and reflecting surface elements in V_{free} as:

$$p_{tot}(x_r \in V_{free}) = p_{q0}(x_r) - \sum_{j=1}^{N} p_{s,j}\frac{e^{-jkR_j}}{R_j}\left(jk\beta - \left(jk + \frac{1}{R_j}\right)\left(\vec{e}_{R_j} \bullet \vec{n}_{S_j}\right)\right)\Delta S_j \tag{2.8}$$

2.3.3 2.5D Geometry

Up to this point in the section, the BEM model calculates the pressure in a 2D geometry. This means that the source(s) q_0 are assumed homogeneous in the y-axis, while for example the Nord 2000 rail propagation model proposes the use of an infinite incoherent line source.

In order to enable this type of analysis without extending the model into the 3D-plane, a solution proposed by D Duhamel suggests creating a 'pseudo-3D' model or, as it will be referred to in this report, 2.5D model of the problem in question. This is done by assuming the 2D results from equation 2.7 to be homogeneous in the y-axis and applying the following transform:

$$p_{2.5D}\left(x, y, z, k(v)\right) = \frac{1}{2\pi}\int_{-\infty}^{\infty} e^{-j\alpha y} p_{2D}\left(x, z, \sqrt{k^2(v) - \alpha^2}\right) d\alpha \tag{2.9}$$

Where y is the source-receiver distance in the y-axis and p_{2D} is a receiver pressure calculated from equation 2.7. To obtain equivalent levels as the train passes, an angular factor can be introduced to account for the source-receiver distance in the 2.5D space by

$$R(\Theta) = R_0 \tan\frac{\Theta\pi}{180} \quad \text{(m)} \tag{2.10}$$

where R is the the source-receiver distance at the angle Θ of the source XYZ-position in relation to a receiver point in the XZ-plane and R_0 is the source-reciever distance in the XZ-plane.

3
Method

This chapter describes the approach used to achieve the stated aim of the report. In summary the methodology used has consisted of 1 - conducting measurements related to the impedance of train tracks. 2 - replicating the measurement setup used in measurments in the 2.5D BEM model, and tuning the impedance model parameters based on the results from the measurments. 3 - using the chosen impedance parameters in a BEM model corresponding to different measurements conducted of trains with and without LHNS, i.e. predicting the effect of LHNS.

3.1 Ballasted train track impedance study

This section describes the method used for determining the impedance of the ballasted train track surfaces.

3.1.1 Impedance validation measurement at Tortuna test site

Measurements were performed on ballasted train tracks in order to capture the influence of the train track impedance on incident sound.

Equipment

- 3 microphones - GRAS 146AE
- Loudspeaker - Avantone PRO Active MixCube
- Digital Signal Processor & generator - HEAD acoustics SQadriga III.
- Calibrator - B&K 4231

Time, day and place for measurements

The measurements were carried out around 10:00 - 15:00, 18/4 - 2023 at a test facility provided by the STA used for conducting tests on train-related equipment. The site is located in Tortuna, a town situated a few miles from the city Västerås. The site features a total of 3 parallel train tracks at the chosen measurement position. An overview of the area can be seen in figure 3.1

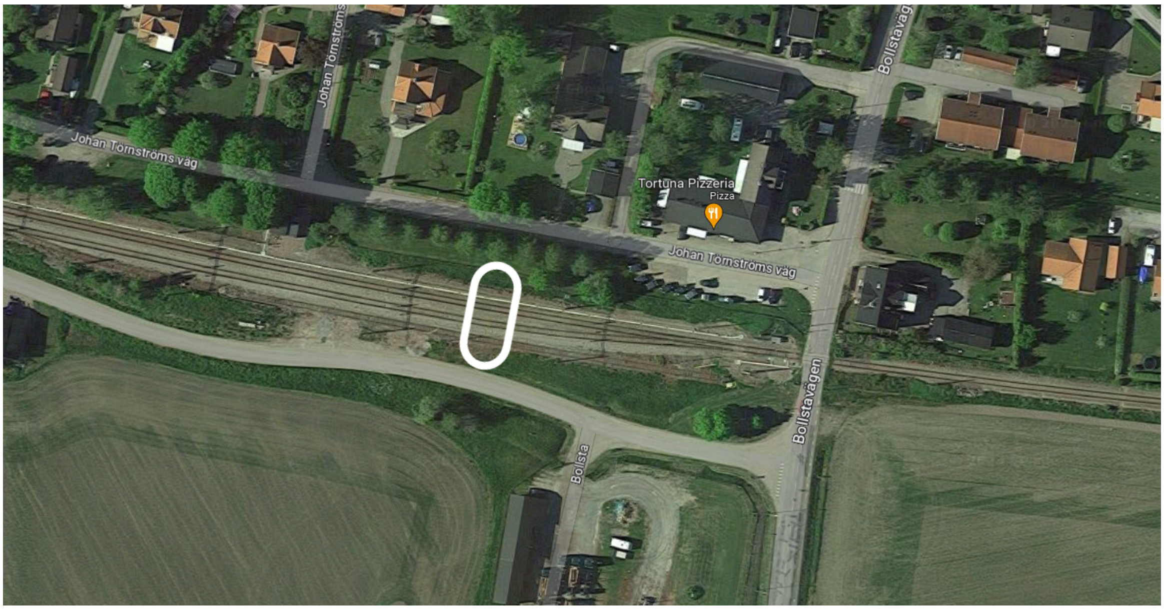

Figure 3.1: *Overview of the measurement site, approximate measurement location is circled in white.*

Meteorological conditions

During the measurement, following meteorological conditions were recorded:

- weak wind: 0-5 $\frac{m}{s}$; occasional gusts $\approx 10\ \frac{\mathrm{m}}{\mathrm{s}}$
- temperature: 15 °C
- static pressure: 1038 hPa
- cloud cover: 5%
- precipitation: 0 mm

Operating conditions

The operating conditions were relatively calm, no noticeable events occurred during the measurement excluding some vehicles passing by the road next to the measurement site. Due to relatively short measurement intervals, these events could be prevented from influencing measurement data by avoiding measurements during these events.

Description of measurement site

The train tracks at the test site were of different types. The ballast used, sleeper types, and general construction differed slightly between the different tracks. To illustrate this, a picture taken at the site is displayed in figure 3.2.

Figure 3.2: *Picture of tracks used in measurement. From left to right the individual tracks will be refered to as: Track 3, Track 2, Track 1.*

As can be seen in the figure, the rightmost track (track 1) has ballast with a generally wider diameter and the ballast layer is thicker in comparison to the two other tracks. Additionally, the sleepers are constructed of concrete instead of wood, as is the case in the other two tracks.

Track 1

Track 2

Track 3

Figure 3.3: *Close-ups of the tracks.*

Measurement setup

The measurements utilized 3 microphones for each recording, one of which functioned as a reference microphone for simulating free field response and the other two being placed above the train tracks of interest. For each track measurments were made with microphones on the 'far', 'mid' and 'close' rail in relation to the loudspeaker. This was mainly done in order to provide more reliable validation data for the BEM-modeling, as well to test if the sleepers had any noticeable influence on the frequency response, as well as providing more reliable validation data for the BEM-modeling.

The loudspeaker played a sine sweep (20 Hz - 10 000 Hz) generated by the SQadriga III. All measurements were conducted twice over a minimum time interval of 10 s (5 sine sweeps), data from each measurement file was reviewed in post-processing to ensure minimal influence from background noise. The two measurements were then averaged in the frequency domain. An illustration of the general setup is found in figure 3.4.

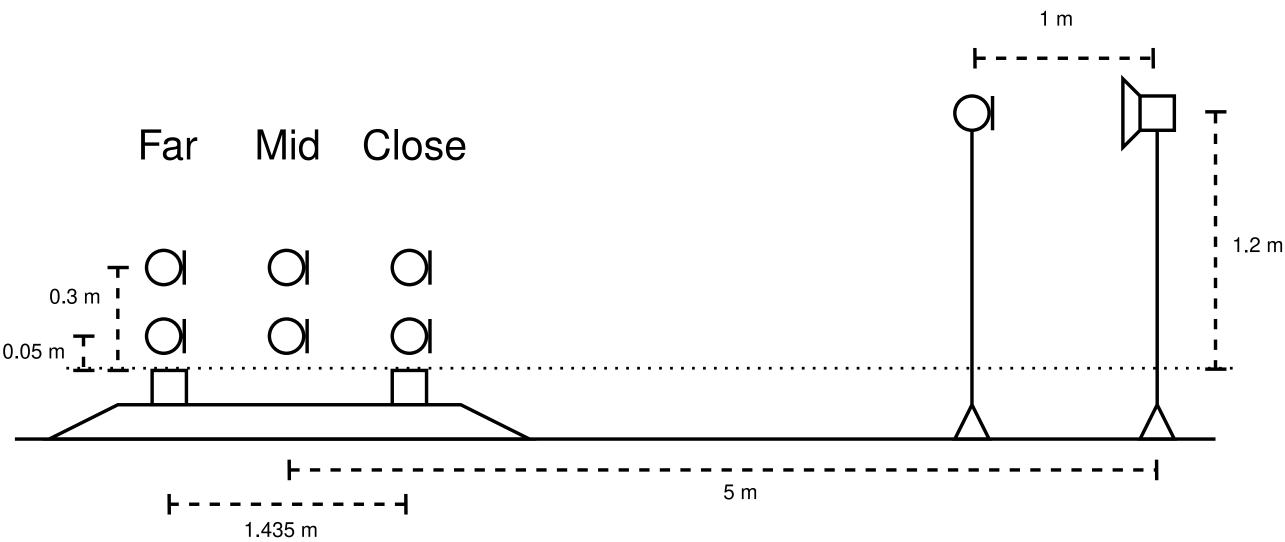

Figure 3.4: *Illustration of the basic measurement setups (not to scale).*

This general setup was applied for 4 different track configurations. In figure 3.5 the 'close' measurement position for each configuration is displayed.

Track 1 - 'rail side'

Track 1 - 'grass side'

Track 2

Track 3

Figure 3.5: *'Close' measurement position setups for all track configurations.*

It is worth mentioning that measurements in accordance with the NORDTEST ACOU 104 [13] report were made for different track parts, but after analysis of the results it was found that the train track surface impedance was too complex to be categorized by this model.

3.1.2 Numerical modeling

In order to run the parameter study for the train tracks, a BEM-model replicating the measurement setups used in Tortuna has been constructed. The geometry of this can be found in figure 3.6. In this figure the source is placed at the same 5 m distance from the rail mid, and 6 different receiver positions are found in the same positions corresponding to the measurement. The rails seen in the figure are modeled to have infinite impedance, while remaining surfaces are modeled with the different finite impedance parameters used in the parameter study. A list of all impedance parameters used can be found in table 3.1

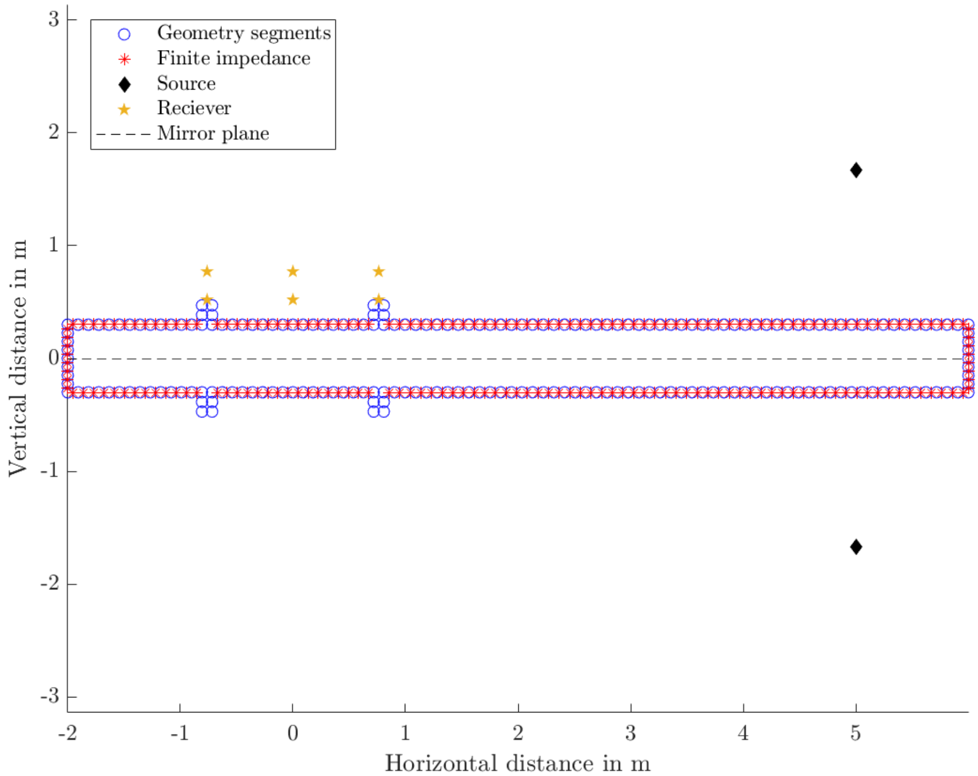

Figure 3.6: *BEM geometry used for the parameter study, the figure shows the lowest element discretization resolution.*

Table 3.1: *Slit-pore impedance model parameters used in each simulation.*

Impedance configuration:	d (m)	σ (Ns/m^4)	ϕ (%)
1	0.30	200	49.1
2	0.30	2000	49.1
3	0.35	200	49.1
4	0.35	2000	49.1
5	0.4	200	49.1
6	0.4	1000	40
7	0.4	2000	49.1
8	0.45	200	49.1
9	0.45	1000	40
10	0.45	1000	49.1
11	0.45	2000	49.1
12	0.5	200	49.1
13	0.5	1000	40
14	0.5	2000	49.1

3.1.3 Data analysis

In order to present the data from measurements and BEM-modeling in a way as to identify the influence of the train track surface impedance, results will be presented in the form of sound pressure level relative to free field.

In the measurement data this is done by subtracting the distance-normalized sound pressure level of the reference microphone from the sound pressure level in each respective microphone position.

$$Lp_{\text{ref, ajusted}} = Lp_{\text{ref}} - 20\log(\frac{R_{track}}{R_{ref}}) \tag{3.1}$$

$$Lp_{re.free} = Lp_{\text{track}} - Lp_{\text{ref, ajusted}} \tag{3.2}$$

Where R_{track} is the distance from source to track microphone, and R_{ref} is the distance from source to reference microphone.

For the numerical modeling this process is done in effectively the same way, although free field results are available for all receiver positions with no need for a reference microphone.

$$Lp_{re.free,BEM} = Lp_{\text{track BEM, direct pressure}} - Lp_{\text{track BEM, total pressure}} \tag{3.3}$$

3.2 LHNS effect study

This section describes the method used for determining the validity of the LHNS IL results from numerical modeling, as well as giving an overview of how the different BEM-models are set up.

3.2.1 Data from previous pass-by measurements with LHNS

In order to validate the effectiveness of the implemented impedance parameters, Measurement data from 3 reports studying the effect of rail-implemented LHNS is used as comparison to the BEM calculation results. Common to all 3 reports is that the measurements are made with trains as a noise source and in more or less the same environment with and without LHNS. The relevant information from the 3 reports will be summarized here.

Quiet City

In this report [14], measurements were performed in 2008 on the same day and general location for both LHNS and non-LHNS. The LHNS used was a Z-Bloc model with track-facing absorber made of rubber and plastic (not vitrumite). The track superstructure (containing 60E1 900A rails, resilient rail pads and monobloc concrete sleepers on ballast) was constructed in accordance to the standard design used in Sweden in 2008. The train pass-by speeds during measurements were approximately 70 km/h. The measurement results are presented in TEL (transit exposure levels), defined as the equivalent sound pressure level L_{eq} during a train passage normalised to the train passage time.

In the report, several different train types are measured and results are given for each type. For the scope of this report 2 train type results are examined;

1. X60 passenger train
2. Industrial train (freight train)

The measurement setup used in the Quiet city report can be seen in figure 3.7, results from mic 3 (w. LHNS) and 4 (w.o LHNS) will be used as validation data in this report. Pictures from the measurement site can be seen in figure 3.8. Measurements were only performed on trains traveling on the LHNS-adjacent track. Data from the relevant measurements are presented in table 3.2.

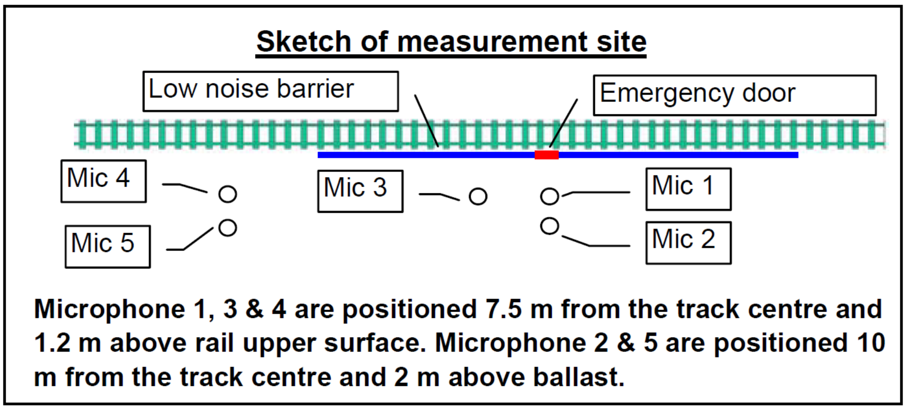

Figure 3.7: *Sketch of Q-city measurement, in this report results from mic 4 and mic 3 are used as validation data [14].*

Figure 3.8: *Location for Q-city measurement [14].*

Table 3.2: *A-weighted TEL measurement results for X60 and industrial train types, w.o LHNS = mic 4, w. LHNS = mic 3.*

Frequency (Hz)	**X60 train (dBA)**		**Industrial train (dBA)**	
	w.o LHNS	w. LHNS	w.o LHNS	w. LHNS
31,5	25	24,9	35,3	34,0
40	29,3	29,1	42,4	42,8
50	38,4	39,9	49,5	50,0
63	46,1	45,9	45,0	43,9
80	45,4	43,4	47,7	46,1
100	46,6	46	51,4	51,3
125	48	46	55,6	55,0
160	53,5	47,1	59,7	57,7
200	57,2	49,6	62,0	58,0
250	55,2	51,5	65,1	62,4
315	61,8	54,8	68,5	65,8
400	66,6	57,4	73,6	70,5
500	64,5	57	75,7	73,8
630	71,5	63,8	79,3	75,5
800	78,2	65,6	82,5	77,9
1000	71,6	63,7	79,2	76,0
1250	68	59,8	74,3	70,3
1600	66,7	59,8	77,0	72,6
2000	65,5	59,3	74,4	70,6
2500	67,2	59,4	76,0	71,8
3150	64,2	57	71,9	67,7
4000	59,1	53,7	67,5	63,9
5000	56,1	51,6	62,8	59,6
6300	55,5	48,4	59,4	56,0
8000	49,7	43,3	54,3	51,0
10000	44,9	39,1	48,6	45,4
Total	**81,1**	**71,7**	**87,7**	**83,9**

Nya Östra Skolan

In this report [15], measurements were carried out in Skogås, connected to the construction of a school "Nya Östra Skolan". The measurements were carried out before (2002) and after (2005) implementation of a Z-Bloc LHNS. The measurements were preformed in accordance with NT ACOU 098 [16]. The measurements are presented as A-weighted maximum values, time weighting fast. In this report measurements have been made for trains both on the adjacent and nonadjacent track in relation to the LHNS. Information about train pass-by speed is not disclosed in report, 70 km/h is assumed. Measured train type is not explicitly stated in the report, but can be assumed to be some sort of passenger train.

Exact measurement positions in relation to railway tracks is not explicitly disclosed in the report, but are approximated to be 25 m from track center, height 1.2 m above top of rail. Data from the relevant measurements are presented in table 3.3.

Table 3.3: L_{AFmax} *measurement results for nya östra skolan.*

Frequency (Hz)	**Northbound train (dBA)**		**Southbound train (dBA)**	
	w.o LHNS	w. LHNS	w.o LHNS	w. LHNS
25	20,5	15,1	21,4	24,4
31,5	25,6	26	26,6	24,5
40	29,6	28,3	32,7	36,1
50	32,2	33,4	34,8	31
63	35,3	30,4	38,4	29,9
80	35,1	27,1	43,1	30,9
100	34,4	30,1	40,2	36,6
125	31,6	34,7	37,3	36,9
160	34,3	39,5	39,7	40,9
200	40,8	40,4	46,5	43,4
250	47,9	43,9	53,3	46
315	49,2	44,2	56,1	48,6
400	52,5	49,2	60,6	52,3
500	52,3	49,1	62,5	54,9
630	54,1	49,6	67,8	60,4
800	65,4	49,1	70,6	54
1000	58,1	49,9	67,4	52,8
1250	54,7	48,7	65,7	53,1
1600	61,4	49,4	68	55,9
2000	56,2	48,2	64,9	52,5
2500	57,5	46	64,9	50,9
3150	55,3	44,2	63	48,3
4000	50,2	40,7	59,6	45,3
5000	45,1	34,2	54,9	39,9
6300	40,6	30,5	50	36,4
8000	34,6	24,4	43,9	32,7
10000	28,9	18,2	37,2	27,4
Total	**69,1**	**59,2**	**76,6**	**65**

Saltsjöbanan

In this report [17], measurements were carried out in connection to Saltsjöbanan, near the facade of a house situated close to the railway. The measurements were carried out before (2012) and after (2013) implementation of an LHNS, model not specified in report. The measurements were preformed in accordance with NT ACOU 098 [16]. The measurements are presented as A-weighted maximum values, time weighting fast. Report states that the measured trains pass-by speed is in the range 30 to 40 km/h. Measured train type is not explicitly stated in the report, but can be assumed to be some sort of passenger train.

Measurement position distance in relation to railway tracks is in the report approximated as 27m. No information about height in relation to train track is given. Pictures of the measurement position can be found in figure 3.9. Data from the relevant measurements are presented in table 3.4.

Figure 3.9: *Pictures of location for Saltsjöbanan reference measurement, Lillängsvägen 43 [17].*

Table 3.4: *Measurement results for Lillängsvägen 43, Saltsjöbanan.*

Frequency (Hz)	**L_{AFmax} (dBA)** w.o LHNS	w. LHNS
25	7,4	16,7
31,5	11,3	20,2
40	22,0	27,9
50	30,0	32,8
63	36,2	39,2
80	43,8	38,7
100	44,1	39,1
125	41,0	37,5
160	45,4	39,3
200	51,1	41,1
250	59,6	45,0
315	60,0	50,7
400	65,3	58,1
500	66,9	55,8
630	69,0	57,3
800	69,6	58,4
1000	65,6	53,4
1250	62,5	49,2
1600	70,8	52,7
2000	66,9	52,0
2500	66,2	50,5
3150	62,2	46,3
Total	**77,4**	**65,1**

3.2.2 LHNS effect numerical modeling

Here the steps taken to obtain BEM-results comparable with above mentioned pass-by measurements are explained.

3.2.2.1 General setup

The general geometrical setups used in all measurement validation simulations are found in figure 3.10. The track center is found at x-coordinate 0. The LHNS is placed 1.73 m from track center, 0.73 m height above top of rail, 0.3 m width.

Sources are placed at heights corresponding to the ones discussed in chapter 2.2 and are labeled as follows;

- Wheel high: 0.7 m above top of rail *(not applicable for X60 model)*
- Wheel low: 0.35 m above top of rail
- Rail: 0.01 m above top of rail

Receivers are placed in accordance with measurement reports. For the results 5 receiver z-coordinates centered around the main z-coordinate are averaged. The x and z coordinates are as follows:

- Q-City: $x = 7.5$ m, $z = 1.2$ m
- Nya östra skolan: $x = 25$ m, $z = 1.2$ m
- Saltsjöbanan: $x = 27$ m, $z = 3.5$ m

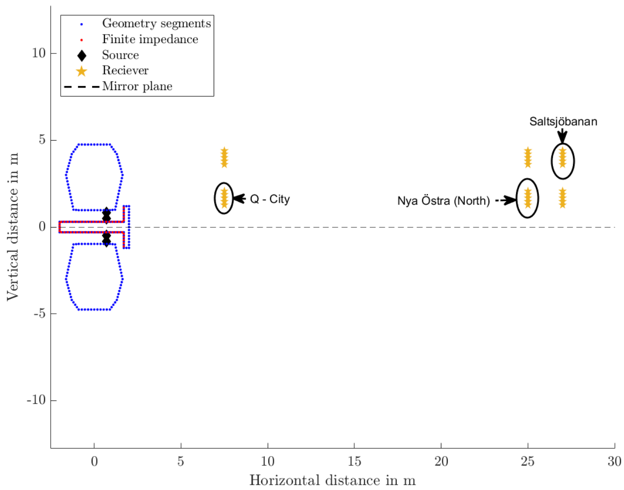

LHNS-adjacent

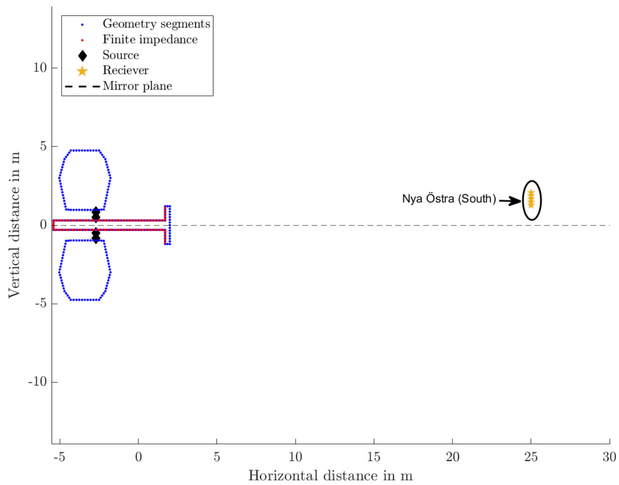

LHNS-nonadjacent

Figure 3.10: *General setup used for all results, in this case the source is a X60 train.*

3.2.2.2 Finite impedance surfaces

Two surface types in the LHNS train model are modeled with finite impedance. The first being the train track surface (labeled Ballast impedance) and the absorptive material 'vitrumite' of the LHNS (labeled LHNS impedance). See fig. 3.11 for an illustration.

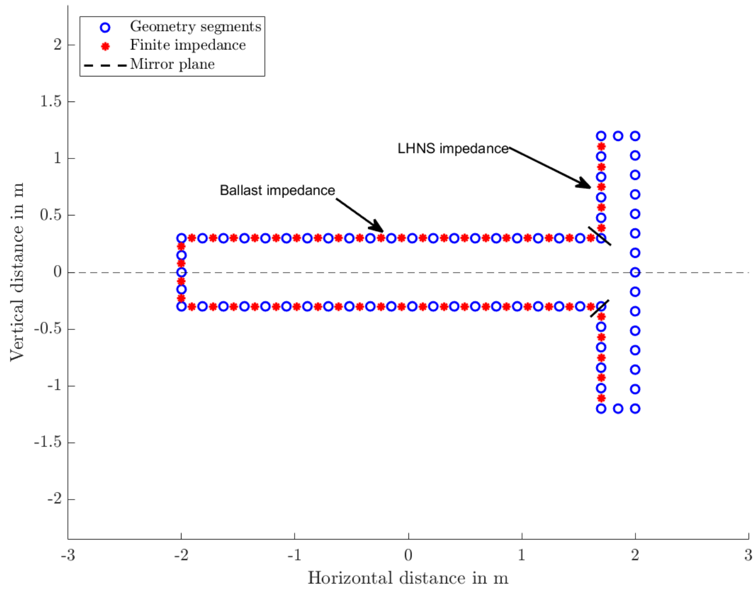

Figure 3.11: *Overview of impedance surfaces.*

The train track surface impedance will be modeled using the Slit-pore impedance model, with parameters based on the findings in section 4.1.2. The LHNS 'vitrumite' surface impedance will be modeled using the Zwikker and Kosten phenomenological porous rigid-frame model, with parameters from the report *Time-domain simulations of low-height porous noise barriers with periodically spaced scattering inclusions* written by Bart van der Aa & Jens Forssén [18]. In the report, an impedance parameter analysis is performed on a layer of vitrumite using impedance tube measurements. The Zwikker and Kosten impedance model parameters used for the LHNS screen in the simulations are presented in table 3.5.

Table 3.5: *Zwikker and Kosten impedance model parameters used for the LHNS screen [18]*

Material:	d (m)	σ (kNs/m^4)	ϕ (%)	k_s (-)
Vitrumite	0.05	29.6	45	2.84

3.2.2.3 Different train type models

Three different railway use-cases will be modelled. The first will be modeled roughly in the shape of a X60 commuter train, the second will be modeled roughly in the shape of an empty industrial wagon, and the third is modeled as an empty track with no train body.

The different models will be displayed in figures 3.12 - 3.14. Note that all illustrative models include multiple sources simultaneously. This is purely for illustrative purposes and in practice simulations are run for the different sources separately.

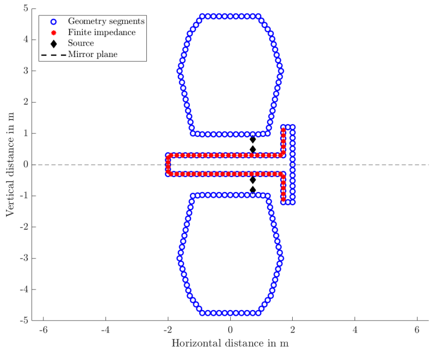

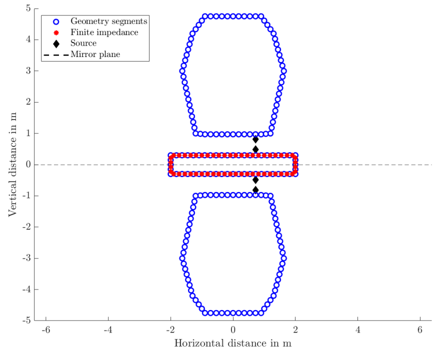

X60 WS 'LHNS - adjacent' *X60 WoS 'LHNS - adjacent'*

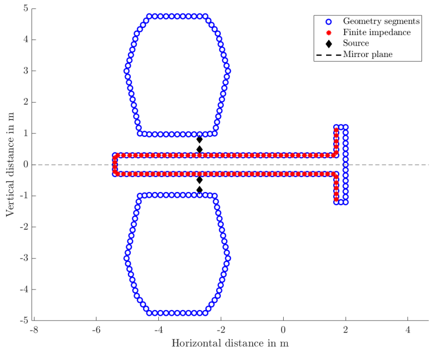

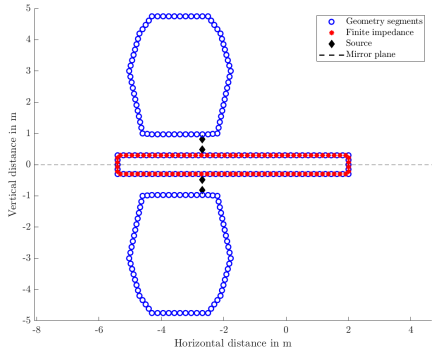

X60 WS 'LHNS - nonadjacent' *X60 WoS 'LHNS - nonadjacent'*

Figure 3.12: *All X60 models used in simulations.*

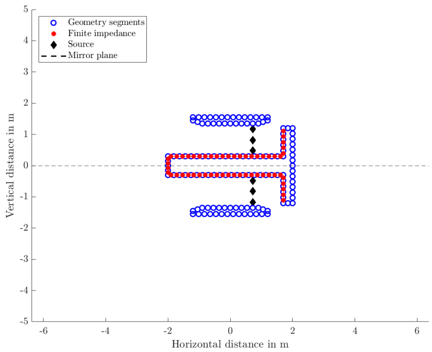

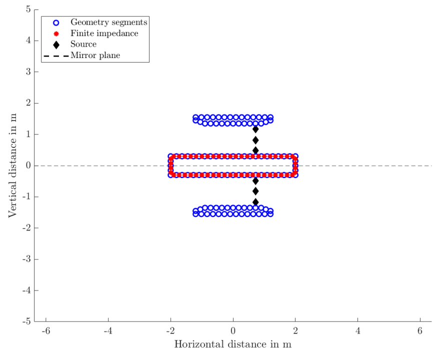

Industrial wagon WS 'LHNS - adjacent' *Industrial wagon WoS 'LHNS - adjacent'*

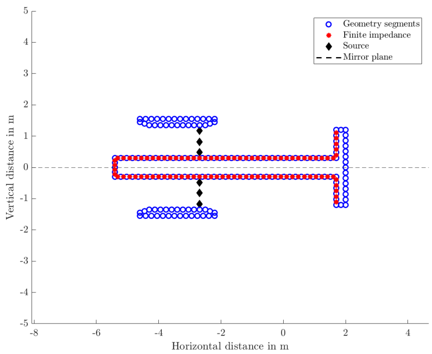

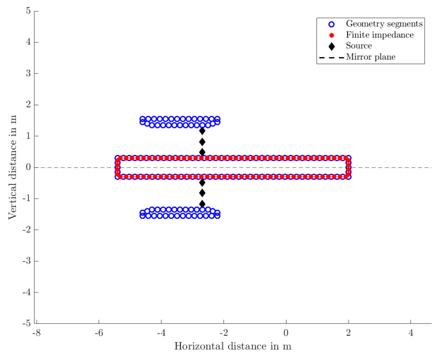

Industrial wagon WS 'LHNS - nonadjacent' *Industrial wagon WoS 'LHNS - nonadjacent'*

Figure 3.13: *All 'industrial wagon' models used in simulations.*

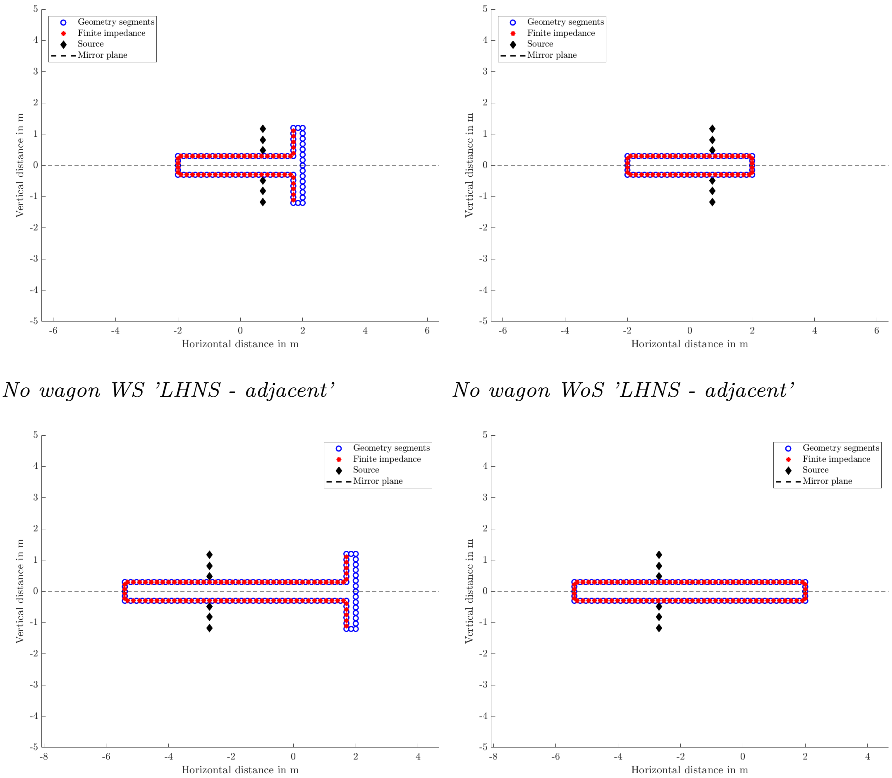

No wagon WS 'LHNS - adjacent' *No wagon WoS 'LHNS - adjacent'*

No wagon WS 'LHNS - nonadjacent' *No wagon WoS 'LHNS - nonadjacent'*

Figure 3.14: *All 'no wagon' models used in simulations.*

3.2.3 Data analysis and post processing

In order to make the calculated pressure results from the BEM simulations comparable with measurement data, some post-processing is necessary. Firstly the relative source power distribution between the two main sources (rail & wheel) has to be estimated. This is done by calculating weighting coefficients based on the sound power measurements performed in [12] for X2000 trains. The operation is performed by calculating the relative contribution of power based on figure 2.6.

$$R_w(f) = \frac{W_{0,rail}(f)}{W_{0,rail}(f) + W_{0,wheel}(f)} \quad (-) \tag{3.4}$$

$$W_w(f) = \frac{W_{0,wheel}(f)}{W_{0,rail}(f) + W_{0,wheel}(f)} \quad (-) \tag{3.5}$$

Where R_w and W_w are the weighting coefficients for rail and wheel while W_0 denotes sound power from fig. 2.6. The calculated values of R_w and W_w for trains travelling at 40 km/h and 70 km/h are presented in figure 3.15.

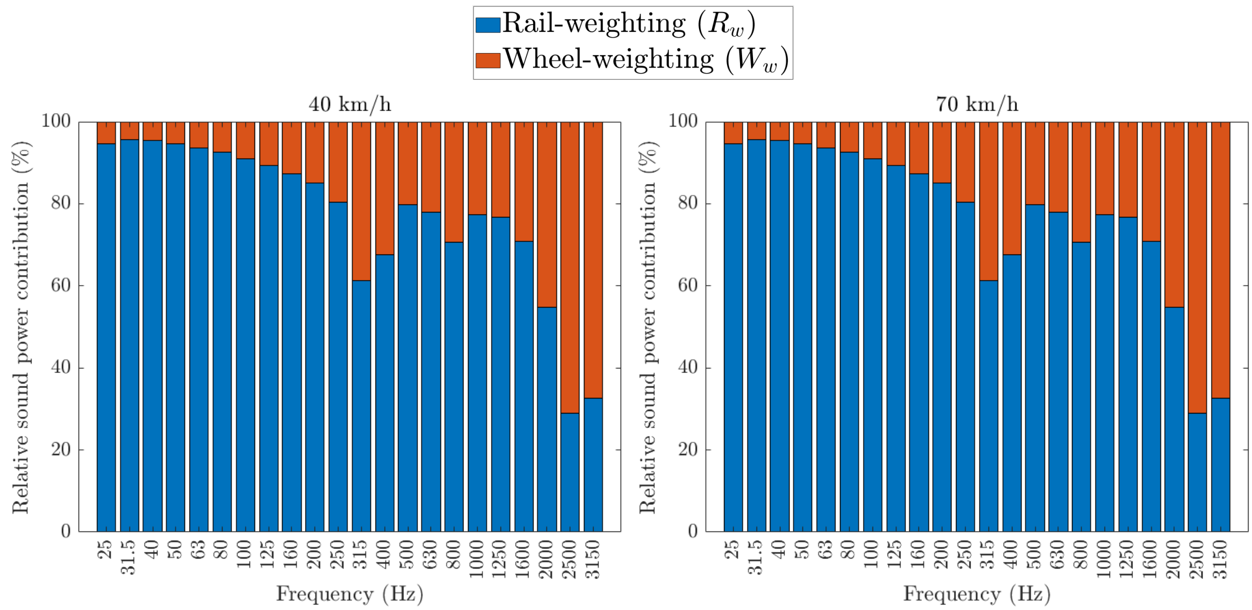

Figure 3.15: *Calculated weighting coefficients for rail / wheel source position.*

Total sound pressure energy from both the rail and wheel source can then be expressed as

$$|p_{0,Ew}(f)|^2 = R_w(f)\,|p_{0,\mathrm{rail}}(f)|^2 + W_w(f)\,|p_{0,\mathrm{wheel}}(f)|^2 \quad \text{(Pa)}$$

where $p_{0,Ew}$ is the energy-weighted (**Ew**) pressure calculated in BEM from each of the sources.

Secondly, since the available validation data exists in both equivalent and maximum levels, two distinct data sets are required. The equivalent pressure is assumed to be an average of all sound incident angles Θ generated by the train in the 2.5D BEM model. This is computed by

$$L_{p,BEM,Ew,Deq} = 10 \times \log 10 \left(\frac{1}{N_d} \sum_{n}^{Nd} |p_{0,Ew,n}|^2 \right) \quad \text{(dB)} \tag{3.6}$$

where n is the index of each angle and N_d is the number of angles in $p_{0,Ew}$. The maximum pressure level is assumed to occur when the source-receiver distance is minimal. In other words at:

$$L_{p,BEM,Ew,0^\circ} = 10 \times \log 10 \left(|p_{0,Ew,0^\circ}|^2 \right) \quad \text{(dB)} \tag{3.7}$$

The LHNS IL is then calculated by subtracting the energy-weighted sound pressure level without screen (**WoS**) with the corresponding results with screen (**WS**) for each case.

$$IL_{Ew} = L_{p,BEM,Ew,WoS} - L_{p,BEM,Ew,WS} \quad \text{(dB)} \tag{3.8}$$

Due to the fact that the BEM-model assigns each source as emitting white noise, calculations of total A-weighted IL from LHNS needs to be adjusted to account for the power spectrum of a train. This is done by using the measured levels WoS from the validation data in chapter 3.2.1 as a baseline and subtracting the corresponding BEM-simulated IL_{Ew} results.

$$L_{p,Ew,WS} = L_{p,measured,WoS} - IL_{Ew} \quad \text{(dB)} \tag{3.9}$$

The total A-weighted sound pressure level for the measured case WoS and the BEM-calculated, spectrum-ajusted WS is then calculated using:

$$L_{pA,tot} = 10 \times \log 10 \left(\frac{1}{N_f} \sum_{m}^{Nf} 10^{\frac{L_{pA,m}}{10}} \right) \quad \text{(dBA)} \tag{3.10}$$

where m is the index of each frequency band in the spectrum and N_f is the number of frequency bands of consideration. The total A-weighted IL for each case is then calculated as:

$$IL_{A,tot} = L_{pA,measured,tot,WoS} - L_{pA,Ew,tot,WS} \quad \text{(dB)} \tag{3.11}$$

4

Results and discussion

In this chapter, the results yielded from the methodology are presented and discussed. There are two main sections of the results. The first section presents the results from the train track impedance measurements and compare the measurements with the corresponding numerical modeling result. Based on this comparison, one set of train track impedance parameters will be chosen for the numerical modeling in section two. The second section uses the chosen impedance parameters in LHNS effect simulations that are then compared with corresponding LHNS measurement data.

4.1 Train track impedance study

In this section, the results from measurement & BEM simulations are presented and compared. The finding form the basis for the final chosen impedance parameter combination used in the LHNS effect simulation models.

4.1.1 Measurement results

Measurement results from all microphone positions, presented in the form of sound pressure level relative to free field, can seen in figure 4.1.

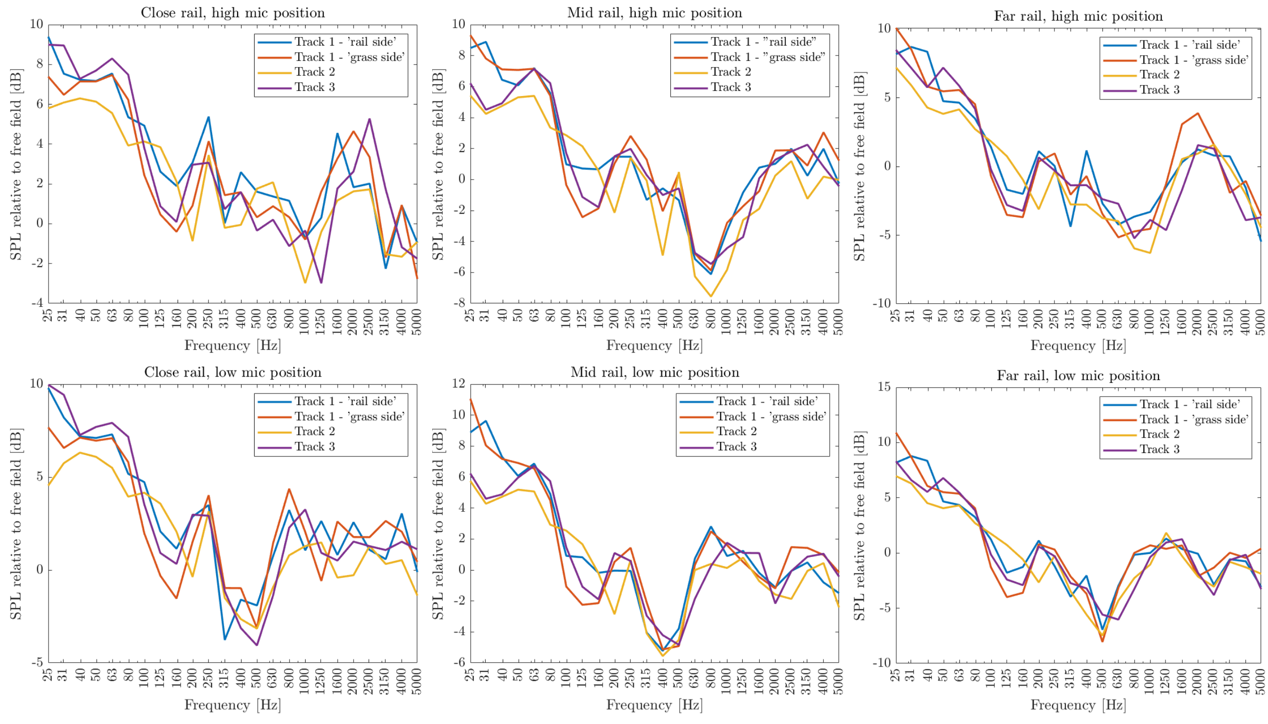

Figure 4.1: *measurement results from tortuna, sound pressure level relative to free field.*

As can be seen in figure 4.1, all track types follow more or less the same trend in all measurement positions, with the exception of track 2 in particularly the first interference dip, being slightly shifted upwards in frequency. The reason for this is unknown but is assumed to be some sort of measurement error. Initially, more pronounced differences were expected between the different track types. Especially in the case of track 1 relative to track 2 and track 3. Notable differences between 'track 2' and other track types are seen, but as discussed this is suspected to be caused by human error. When comparing the different measurement setups in figure 3.3 the expected deviance would arguably be between track 1 and track 2 & 3. Since track 1 is the track type constructed to the current Swedish railway standard, impedance parameters are chosen to fit these measurements best.

4.1.2 Comparison with BEM and choice of parameters

In figure 4.2 results from all numerical simulations are plotted alongside the measurement data.

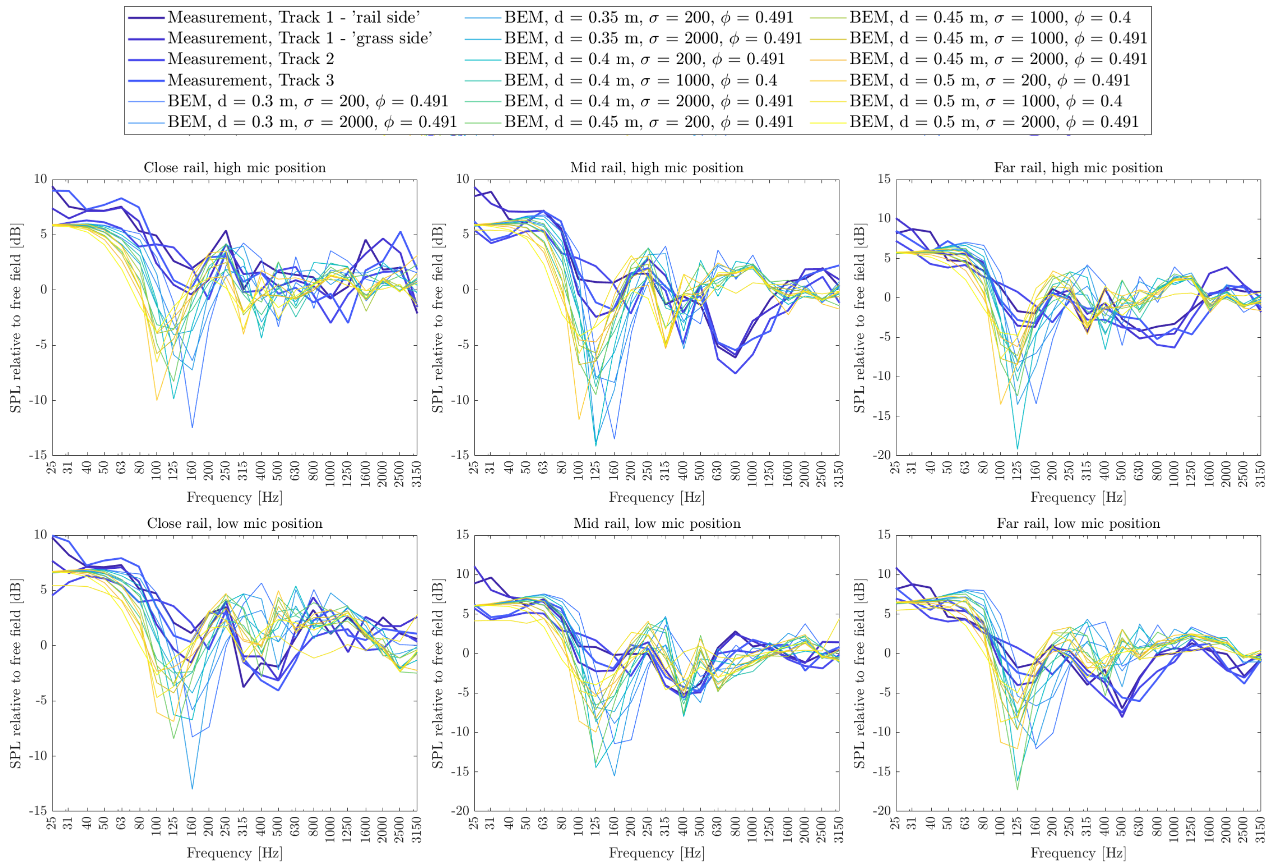

Figure 4.2: *Measurement results from Tortuna, plotted along all 14 impedance parameter configurations.*

As can be seen in figure 4.2, the most notable differences in the modelled results occur in lower frequencies. Overall the simulated results follow the general shape of the measured results below a frequency of 400 Hz, with more or less apparent deviations in the frequency at which the interference occurs. It can also be noted that the first 'dip' of the simulated results are much more pronounced than the measured results. This is likely a result of imperfect measurement conditions, making drastic noise attenuation polluted by background noise. As can be inferred from the numerical modeling results, ballast layer thickness is the parameter with the most prominent influence on the interference patterns.

Chosen parameter combination

The graph for the selected final impedance parameters is plotted alongside measurements in figure 4.3. The impedance parameters for the train tracks are as detailed in table 4.1

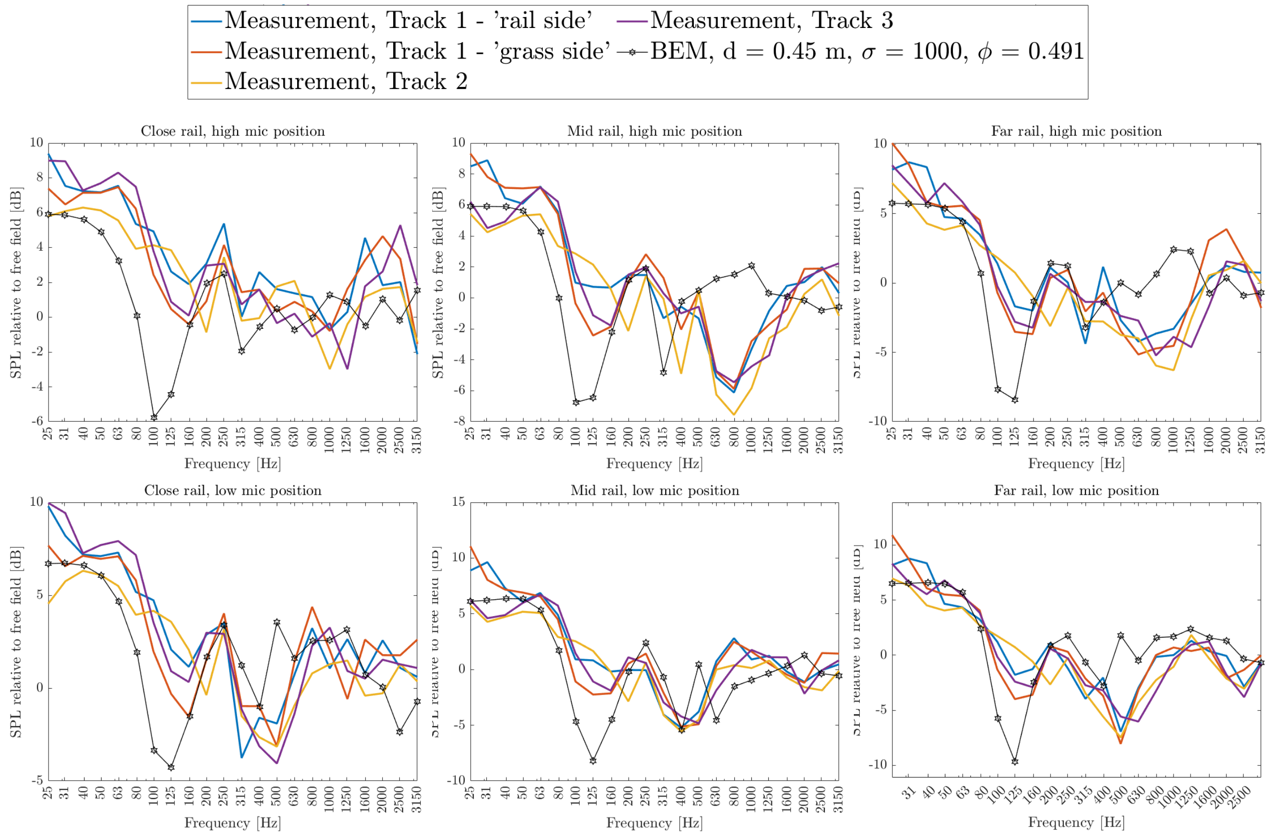

Figure 4.3: *Measurement results from Tortuna, plotted along the chosen impedance parameter configuration.*

Table 4.1: *Slit-pore impedance model parameters used for subsequent train track modeling.*

Material:	d (m)	σ (Ns/m^4)	ϕ (%)
Train tracks	0.45	1000	49.1

The reasoning behind choosing these parameters is that the frequency of the first interference patterns align relatively well with measurements for all positions, more so than any of the other numerical results.

4.2 LHNS effect

In this section results from all train model simulations will be presented. IL results will be presented for all available source positions along with energy weighted (Ew) results in the first graph of each page. In the second graph energy weighted IL results are compared with existing measurement data as well as corresponding results from previous BEM-model iteration results. Additionally, energy weighted sound pressure levels for simulated cases with and without LHNS will be displayed along with corresponding data from measurements. More focus will be put on simulations that can be accurately compared with real world measurements, i.e. X60 simulation models and industrial wagon models in the Q-city setup.

After results from all frequency spectra have been presented, total A-weighted single-number IL results for all energy weighted BEM results along with corresponding values from measurements and previous BEM iteration results are presented and discussed.

4.2.1 X60

Results from all simulation setups using X60 train geometry. Measured results are obtained from a geometrically comparable source to simulated results for all cases.

4.2.1.1 QCITY

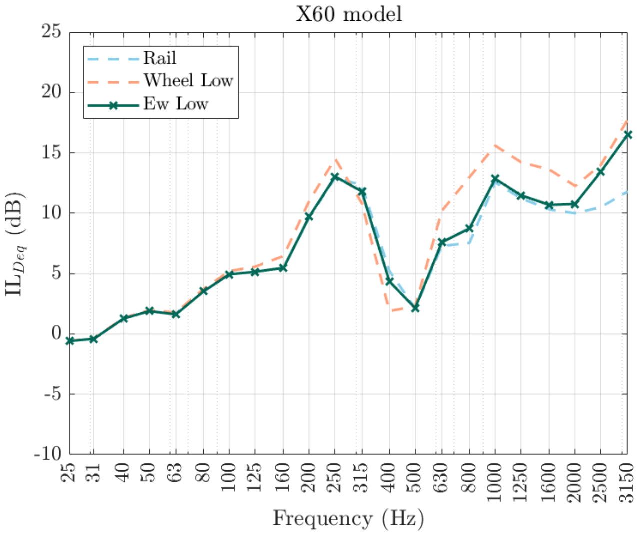

All current BEM results.

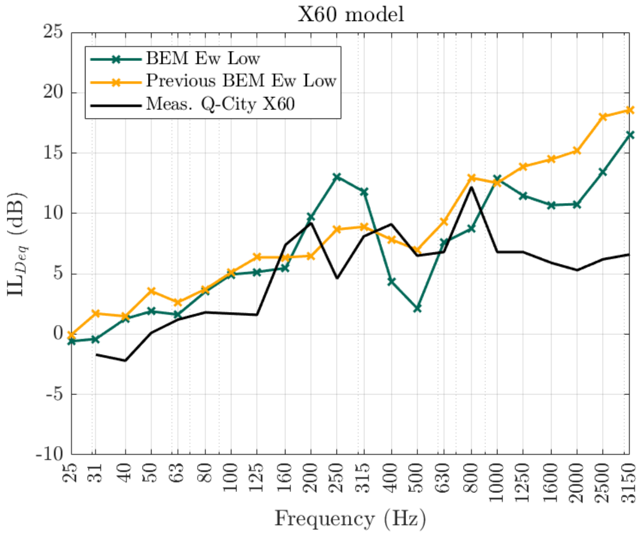

Current and previous Ew BEM results compared to measurement.

Figure 4.4: *IL results from the Quiet City model configuration.*

When comparing the BEM Ew IL results with previous results it is worth noting the large deviations in frequency band 250 Hz and 500 Hz that occur. The local maximum seen at frequency band 800 Hz in the measurement and previous BEM results is shifted to 1000 Hz in the current BEM model results.

In figure 4.5 it is worth noting that the previous BEM results generally align more closely with measured results in frequency bands below 1000 Hz. Above 1000 Hz the current BEM results align more closely with measured results.

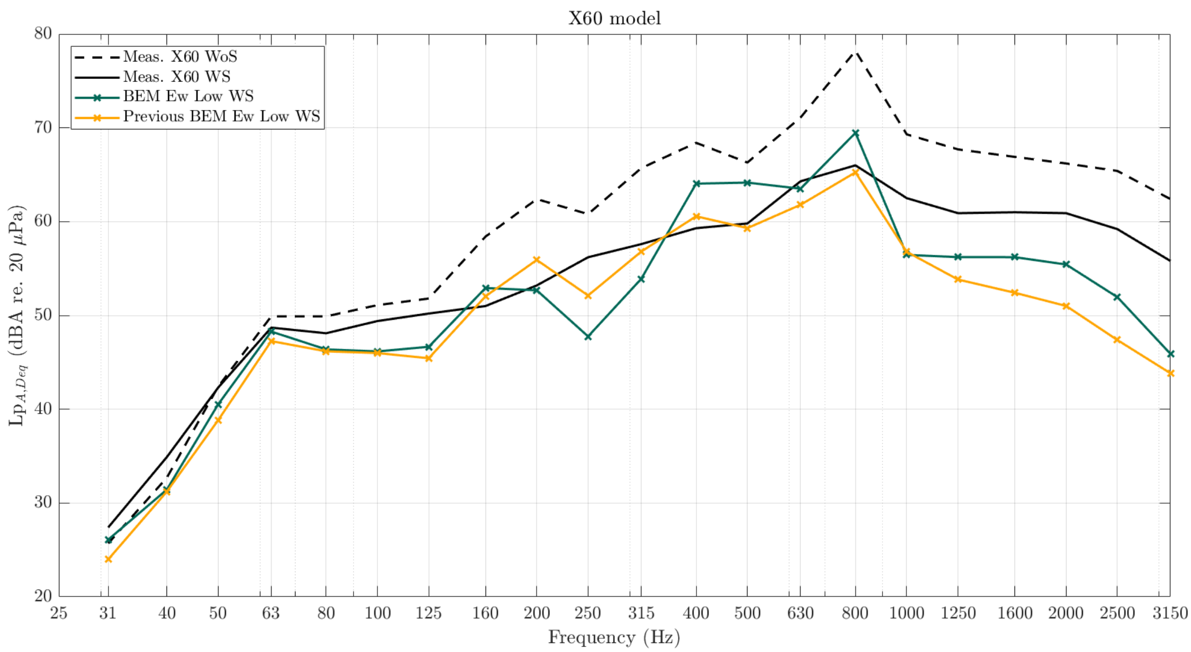

Figure 4.5: *Sound pressure level results from the Quiet City model configuration (calculated from the X60 measurement).*

4.2.1.2 Nya Östra Skolan

Note that Nya Östra Skolan comprises two separate simulation results. One where the train is traveling on the track adjacent to the LHNS, and one where the train is traveling on the track non-adjacent to the LHNS.

LHNS - adjacent track (North)

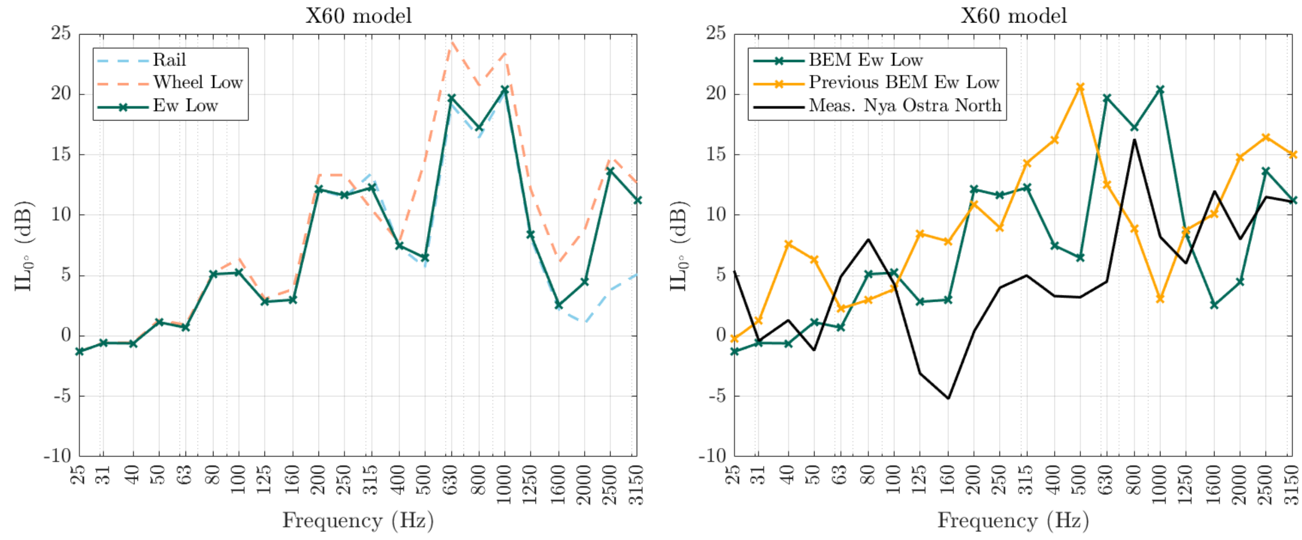

All current BEM results.

Current and previous Ew BEM results compared to measurement.

Figure 4.6: *IL results from the Nya Östra Skolan (North) model configuration.*

When comparing the BEM Ew IL results in figure 4.6 with previous results it is worth noting that the the trends of the IL follow measurements more closely, except in the 1600 Hz frequency band.
In figure 4.7 it can be seen that the discrepancy between measured and BEM IL in the 1600 Hz frequency band materially impacts the total WS results for the current BEM model, while the previous BEM model has the same problem in the 1000 Hz frequency band.

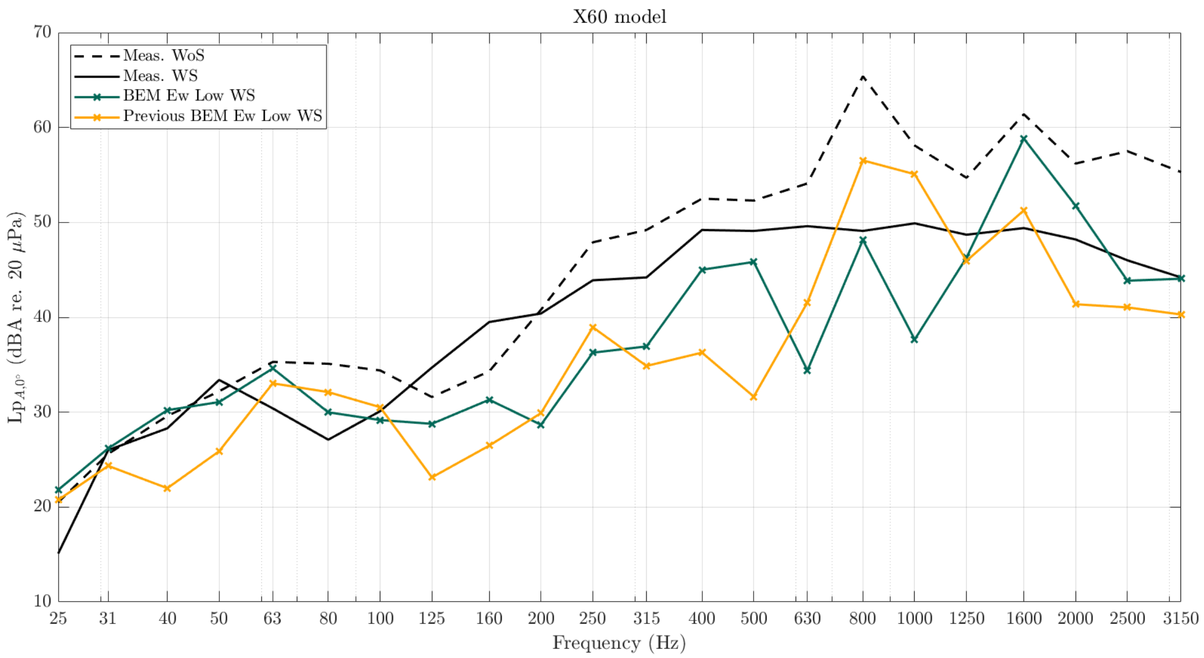

Figure 4.7: *Sound pressure level results from the Nya Östra Skolan (North) model configuration.*

LHNS - nonadjacent track (South)

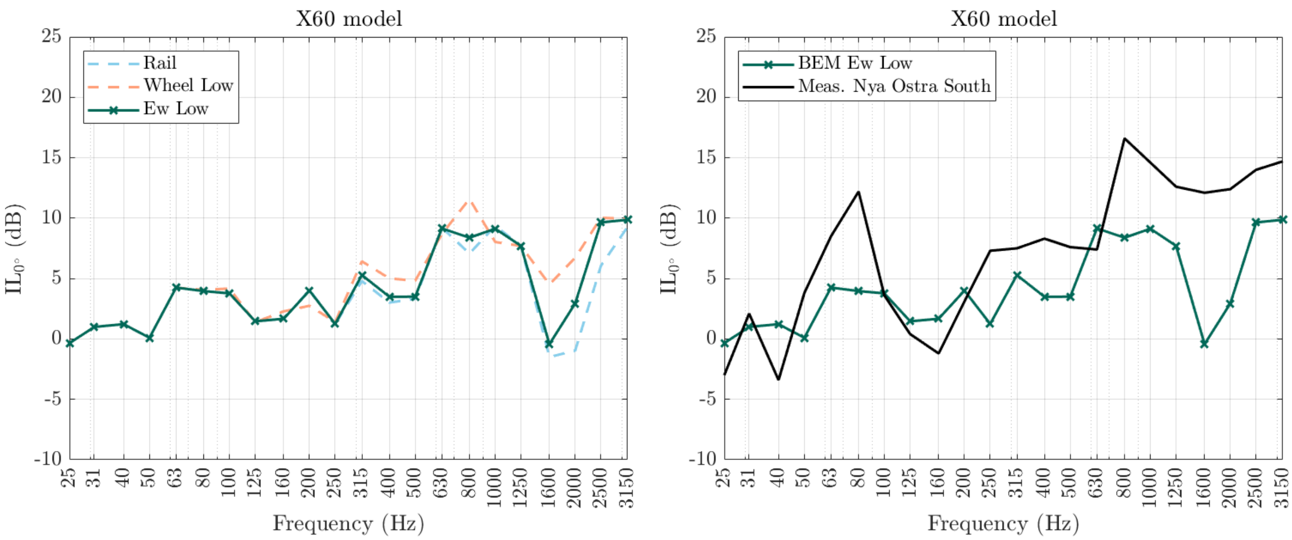

All current BEM results. *Current Ew BEM results compared to measurement.*

Figure 4.8: *IL results from the Nya Östra Skolan (South) model configuration.*

When observing the results in both figure 4.8 and 4.9 it can be seen that general trends in IL results are somewhat accurate to measurements, however, just as in the LHNS-adjacent track configuration the 1600 Hz frequency band creates a substantial discrepancy in the total WS results. Closer examination of figure 4.8 shows that this discrepancy is less severe when only considering the Wheel Low source position.

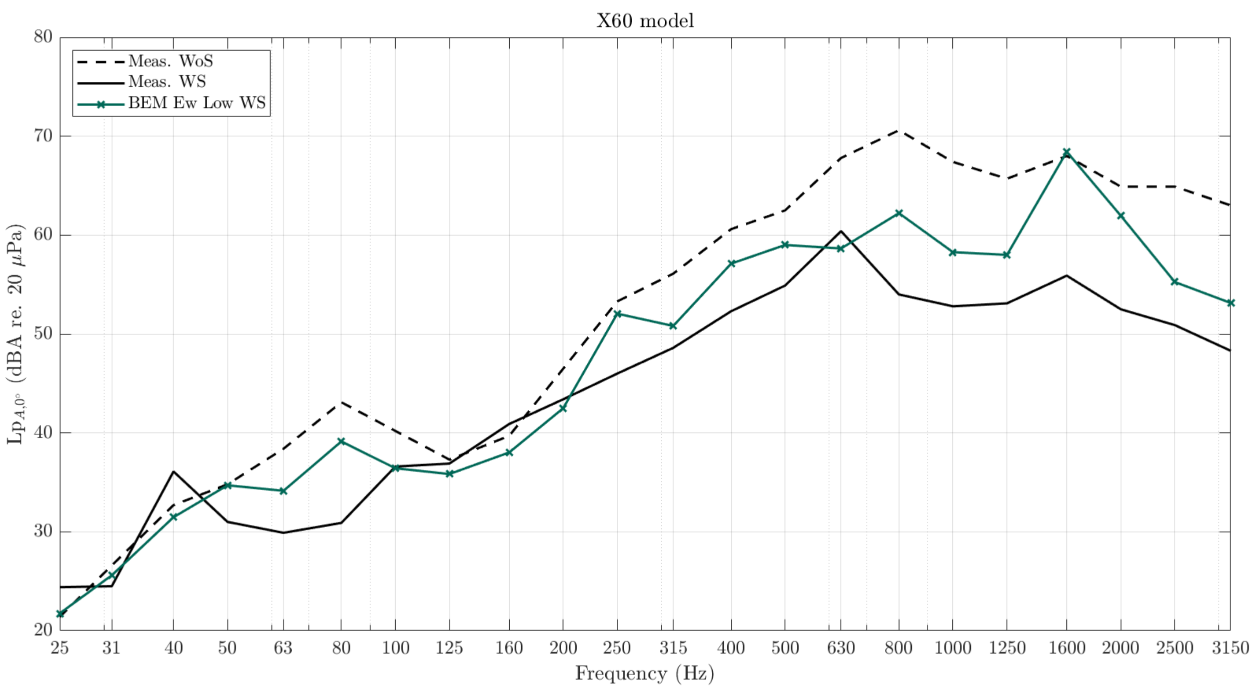

Figure 4.9: *Sound pressure level results from the Nya Östra Skolan (South) model configuration.*

4.2.1.3 Saltsjöbanan

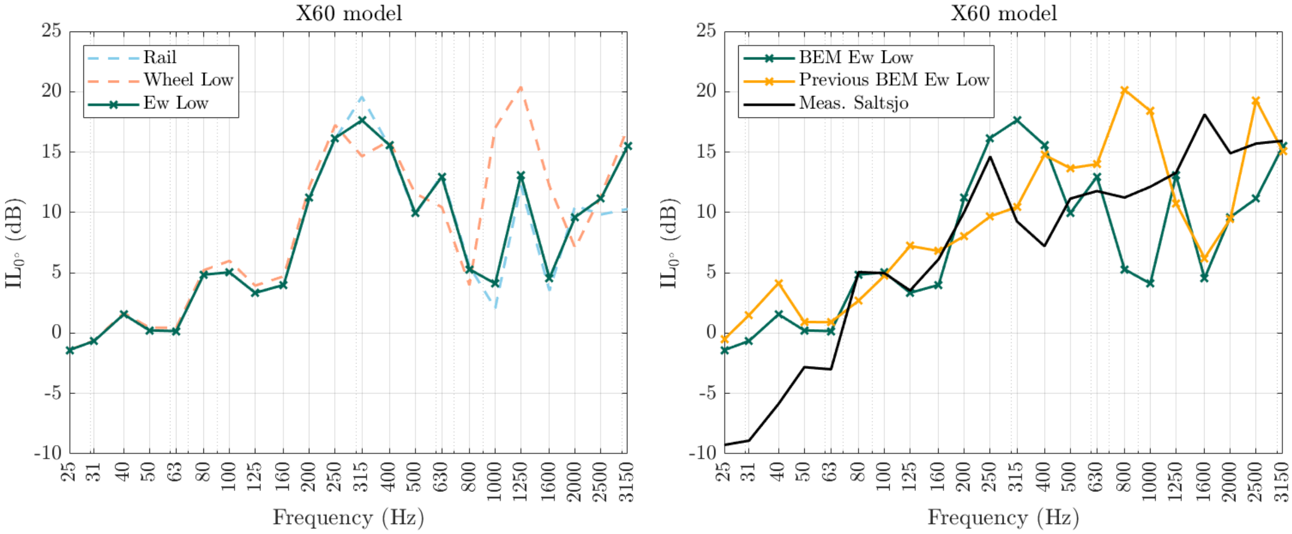

All current BEM results.

Current and previous Ew BEM results compared to measurement.

Figure 4.10: *IL results from the Saltsjöbanan model configuration.*

When comparing the BEM Ew IL results with previous results in figure 4.10 it is worth noting that the IL peak at 250 Hz in the measurement is more represented in the current BEM results. Additionally, when comparing the Rail and Wheel Low result it can be seen that the apparent IL peak in the measurement at 1600 Hz is more represented in Wheel Low results.

When comparing the sound pressure level between the BEM-calculated and measured results in figure 4.11 it can be seen that the 800 Hz, 1000 Hz and 1600 Hz frequency bands are not accurately represented in the BEM results.

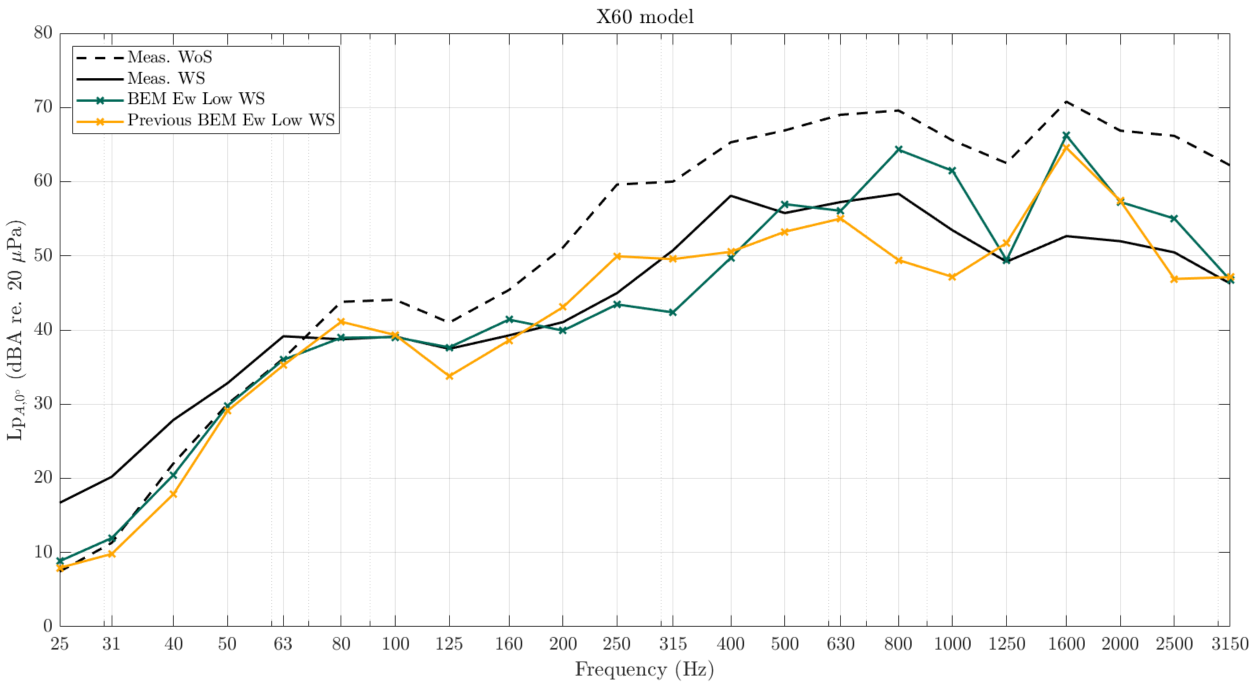

Figure 4.11: *Sound Pressure Level results from the Saltsjöbanan model configuration.*

4.2.2 Industrial wagon

Results from all simulation setups using industrial train geometry. Measured results are obtained from a geometrically comparable source to simulated results only for the Q-City setup.

4.2.2.1 QCITY

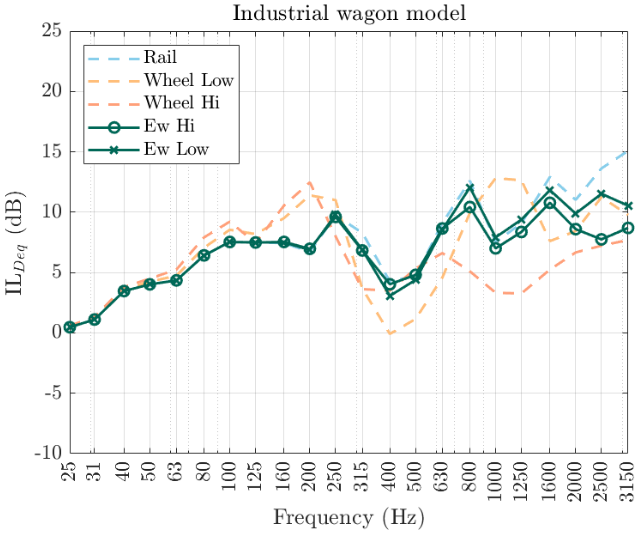

All current BEM results.

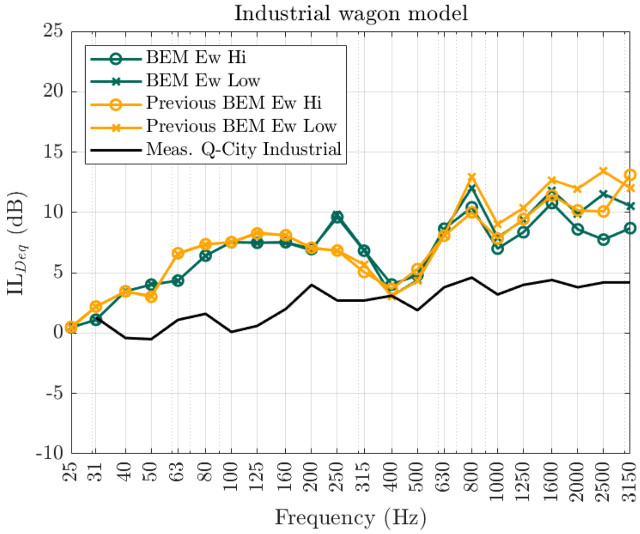

Current and previous Ew BEM results compared to measurement.

Figure 4.12: *IL results from the Quiet City model configuration.*

When comparing the BEM Ew IL results with previous BEM results in figure 4.12 it can be seen that the results are more or less the same, apart from the IL peak at 250 Hz. It is also worth noting that the Wheel Hi results are somewhat more consistent with measured results in frequency bands above 250 Hz, while the Rail results are more consistent below 250 Hz.

When observing figure 4.13 it can be noted that the simulated WS results generally follows the trend of the measured WS results. The simulated results however overestimate the IL effect of the LHNS over the entire spectrum, except in the 400 Hz frequency band.

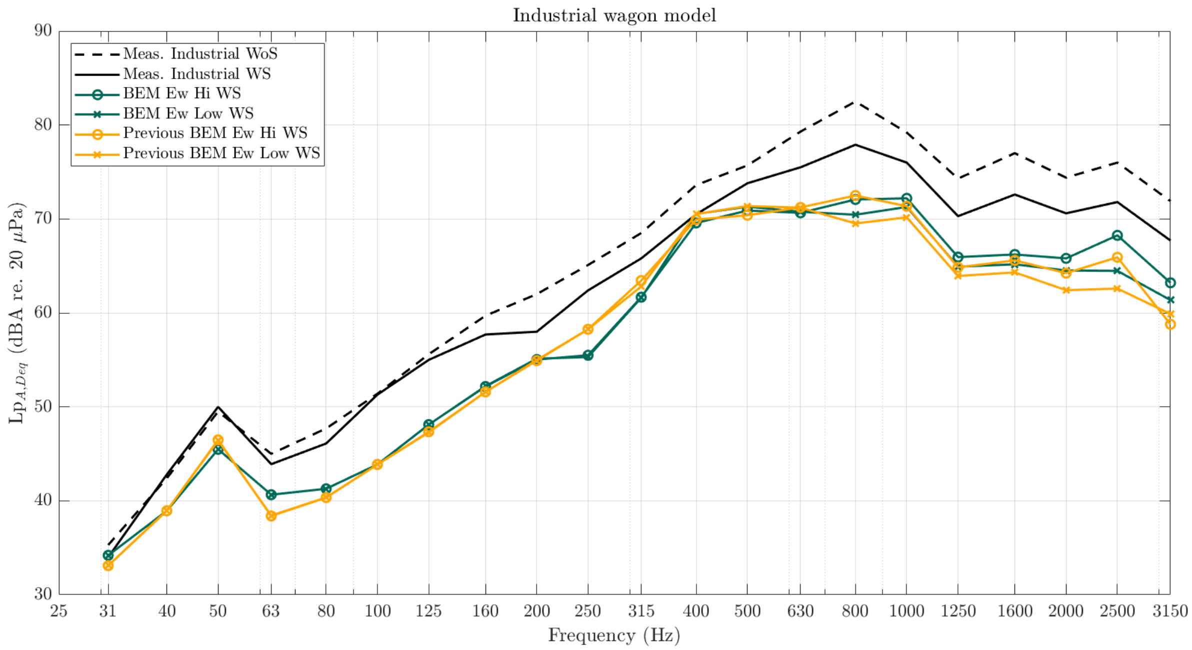

Figure 4.13: *Sound Pressure Level results from the Quiet City model configuration (calculated from the industrial train measurement).*

4.2.2.2 Nya Östra skolan

LHNS - adjacent track (North)

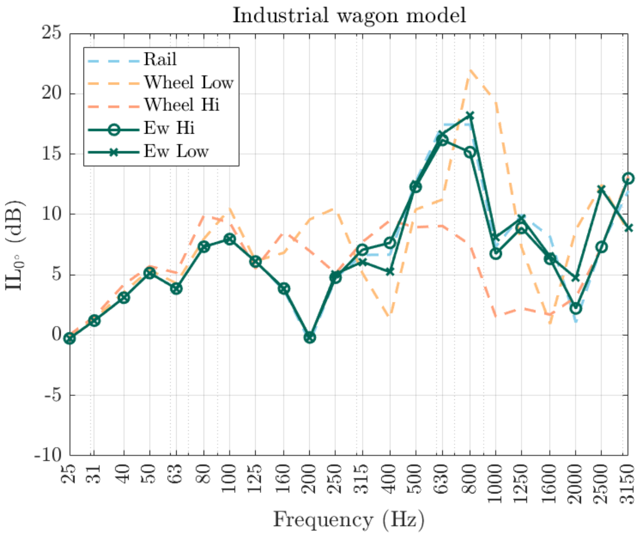

All current BEM results.

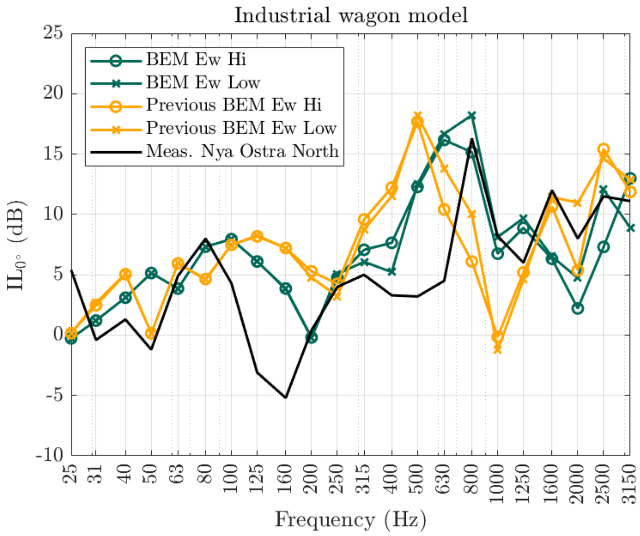

Current and previous Ew BEM results compared to measurement.

Figure 4.14: *IL results from the Nya Östra Skolan (North) model configuration.*

In figure 4.14 note the large differences between the Wheel Hi & Wheel Low sources and that the low wheel source more closely aligns with the measured results than the high wheel source.

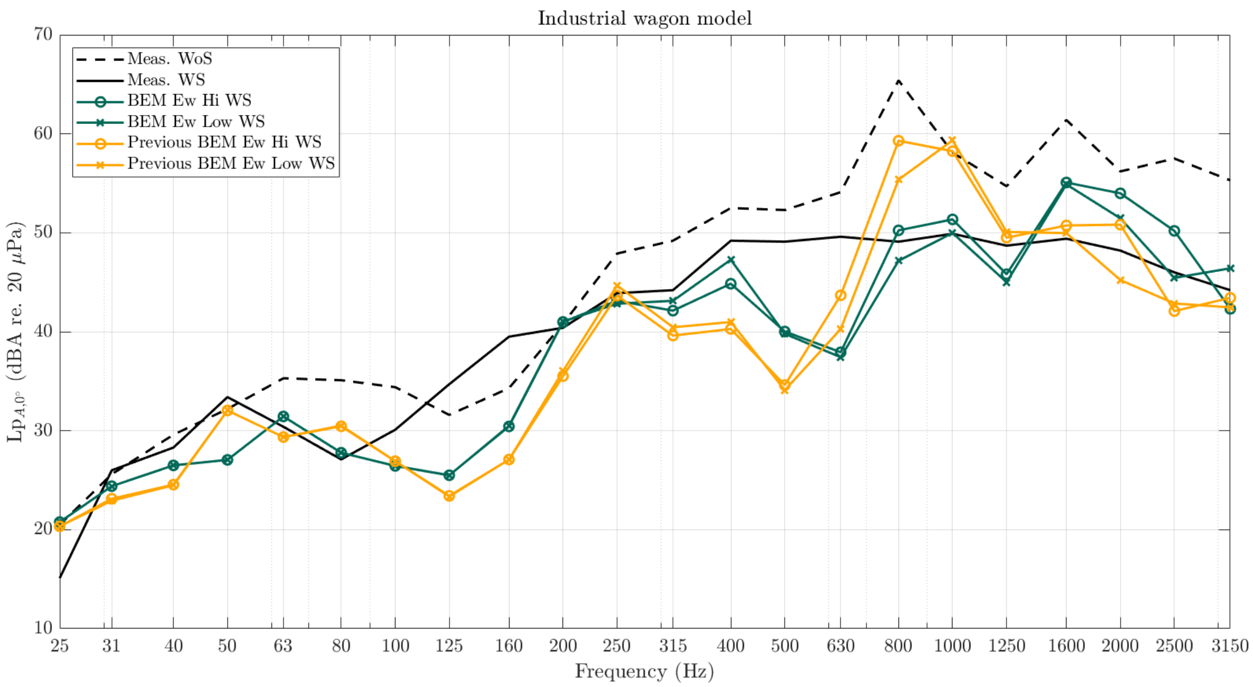

Figure 4.15: *Sound Pressure Level results from the Nya Östra Skolan (North) model configuration.*

LHNS - nonadjacent track (South)

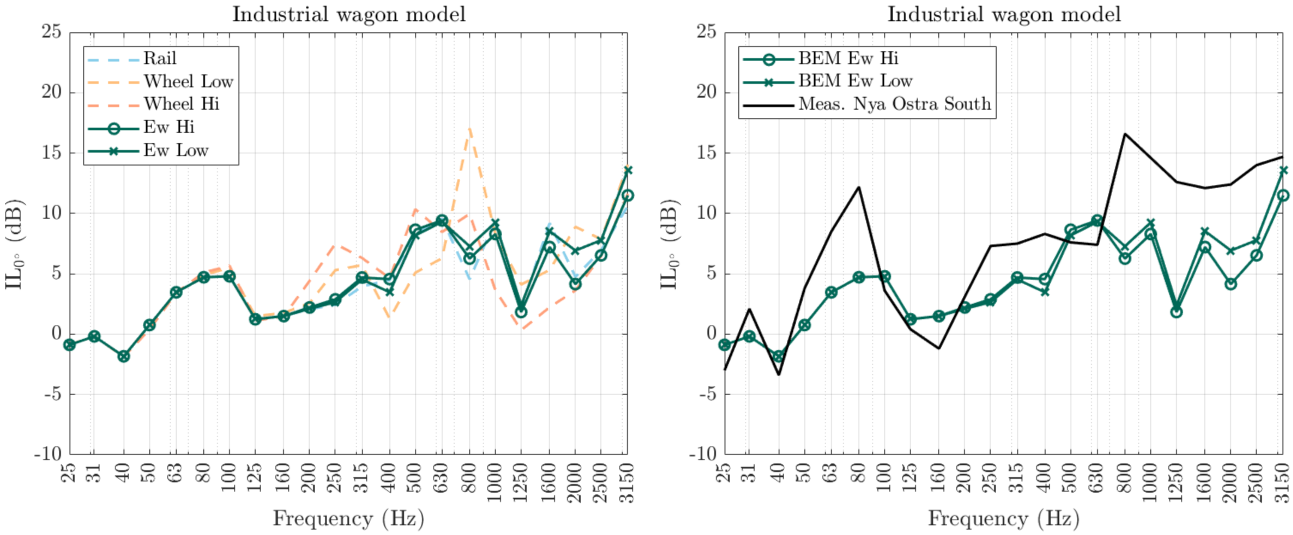

All current BEM results. *Current Ew BEM results compared to measurement.*

Figure 4.16: *IL results from the Nya Östra Skolan (South) model configuration.*

In figure 4.16 note again the large differences between the Wheel Hi & Wheel Low sources and that the low wheel source more closely aligns with the measured results than the high wheel source, particularly in the 800 Hz frequency band.

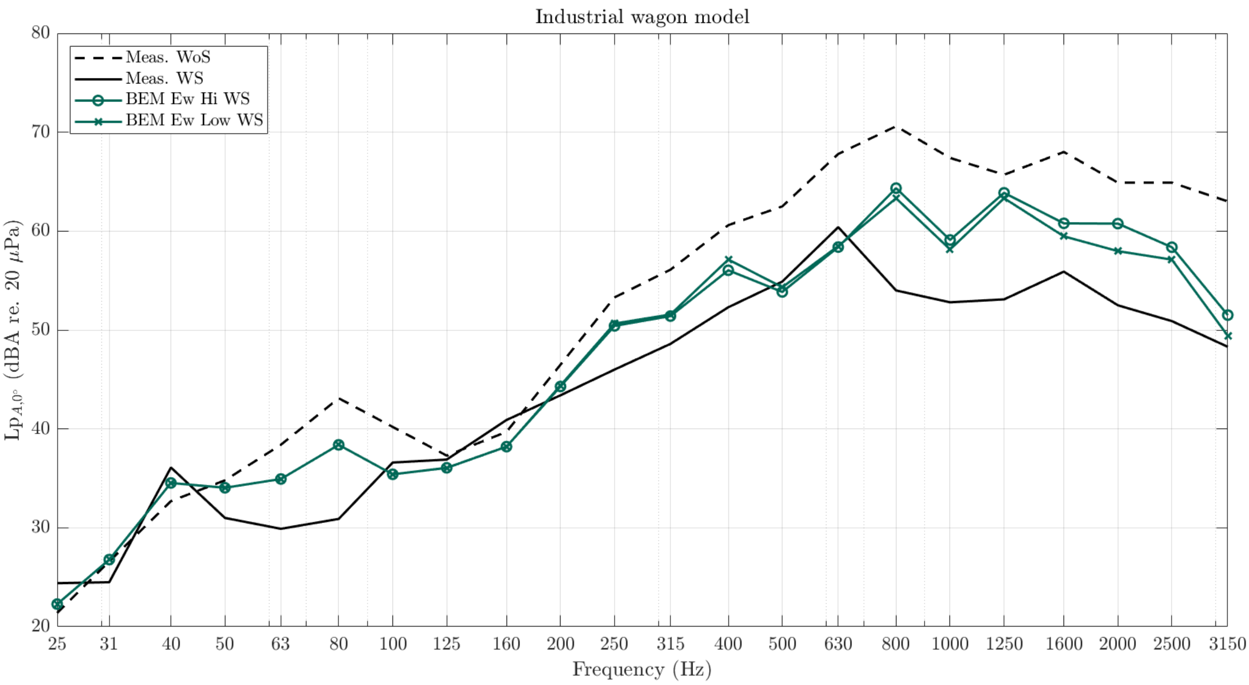

Figure 4.17: *Sound pressure level results from the Nya Östra Skolan (South) model configuration.*

4.2.2.3 Saltsjöbanan

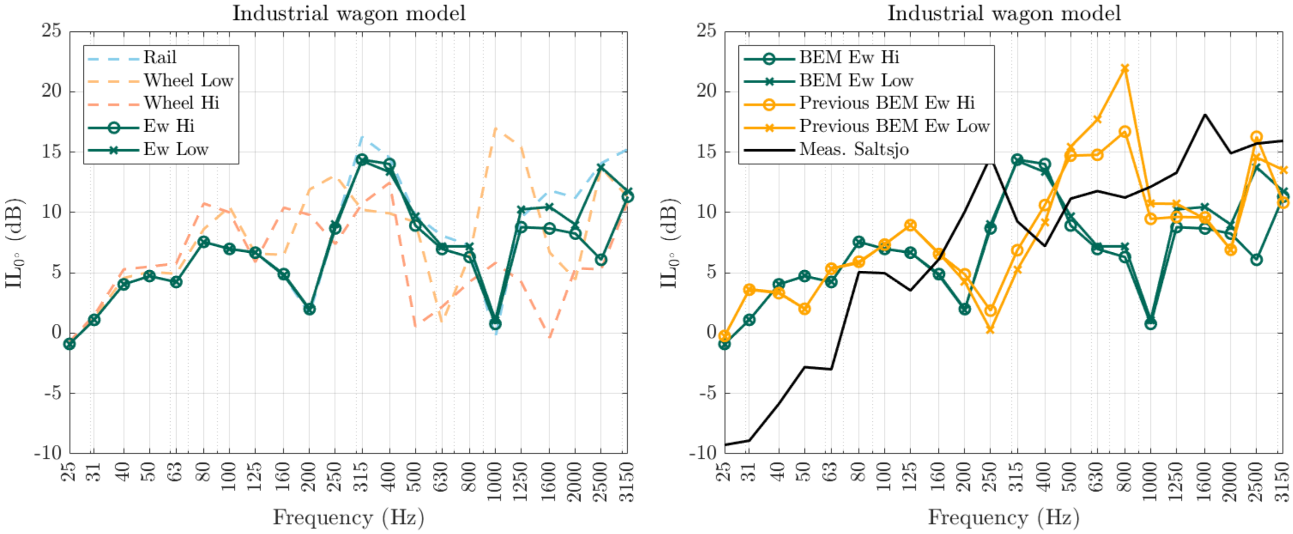

All current BEM results.

Current and previous Ew BEM results compared to measurement.

Figure 4.18: *IL results from the Saltsjöbanan model configuration.*

In figure 4.18 note the significant deviation between previous BEM IL results and current results. Additionally, the Wheel Low source more closely aligns with measured results than the Ew results in the frequency range between 800 Hz and 1250 Hz.

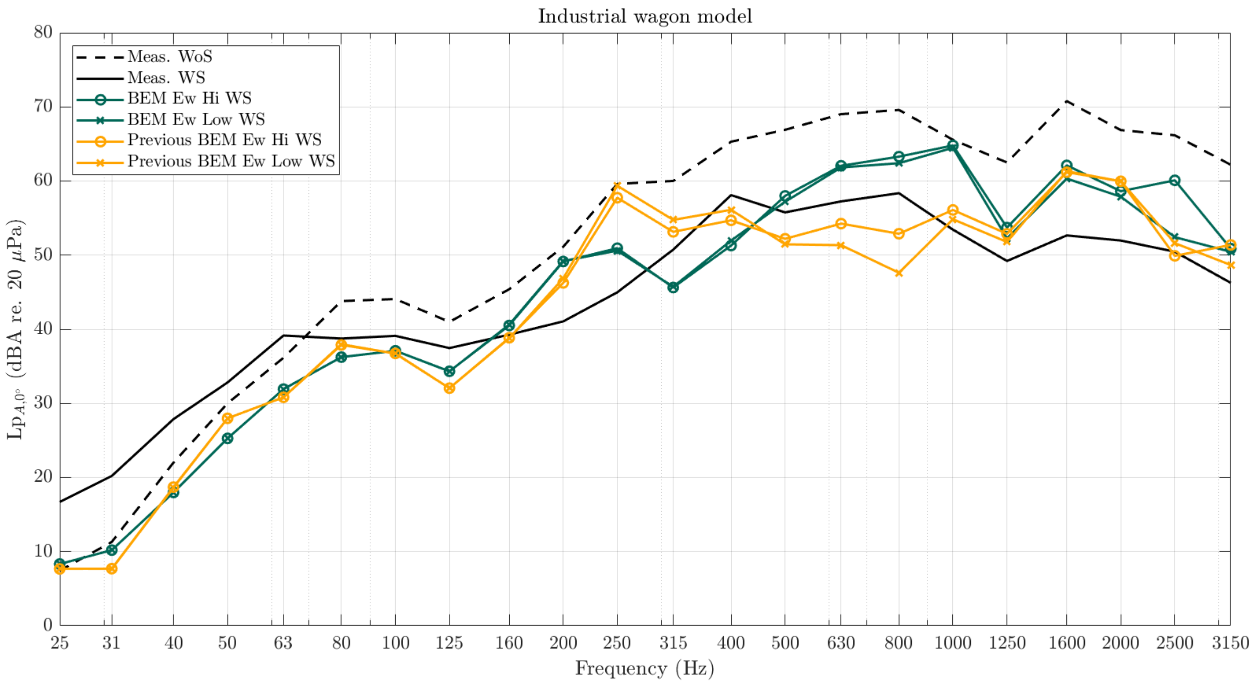

Figure 4.19: *Sound pressure level results from the Saltsjöbanan model configuration.*

4.2.3 No wagon

Results from all simulation setups using no train geometry, only sound source. No directly comparable measurement results exists.

4.2.3.1 QCITY

Note that the sound pressure level spectra will be presented as two figures in this setup, this is because the simulated no wagon results are compared with both available measurement results from the Quiet City report, the X60 and industrial wagon measurements.

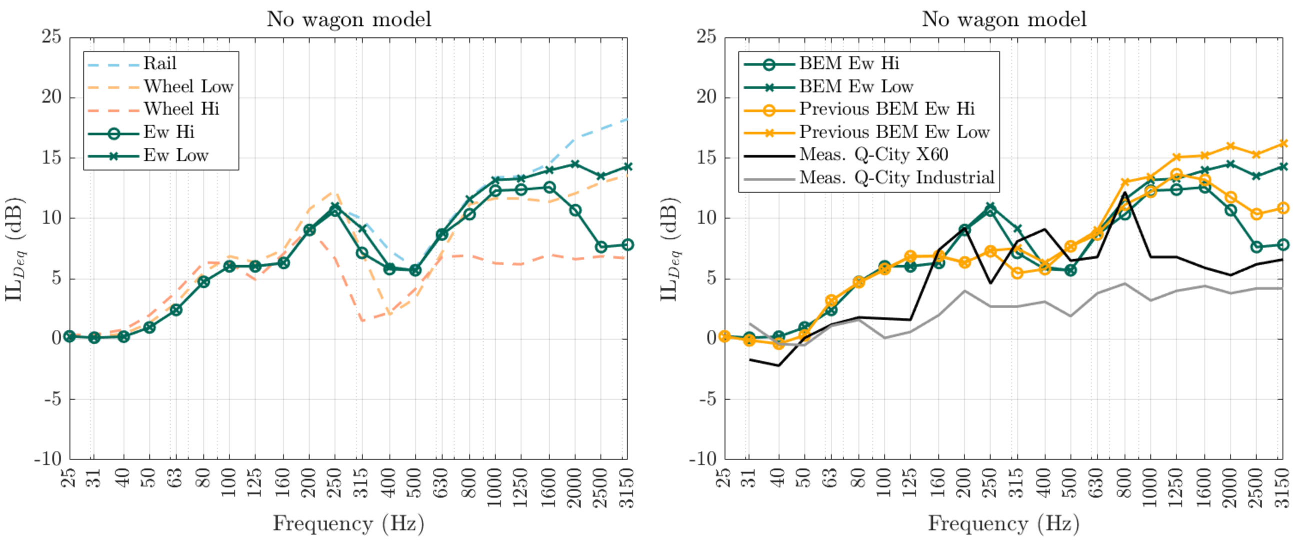

All current BEM results.

Current and previous Ew BEM results compared to measurements.

Figure 4.20: *IL results from the Quiet City model configuration.*

In figure 4.20, note the closer alignment to measured results is the non-Ew high wheel source in frequency bands above 800 Hz as well as in the 250 Hz band. In figure 4.21 & 4.22 the simulated sound pressure level results are presented for both the X60 and industrial train measurements.

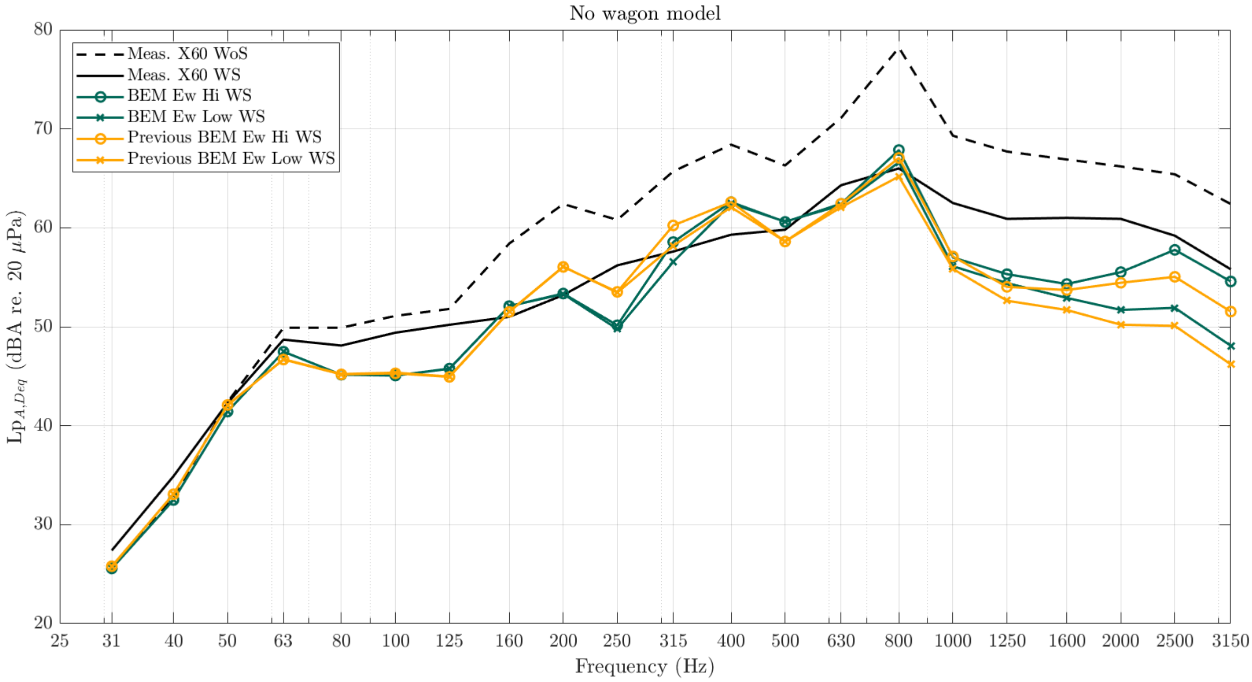

Figure 4.21: *Sound pressure level results from the Quiet City model configuration (calculated from the X60 measurement).*

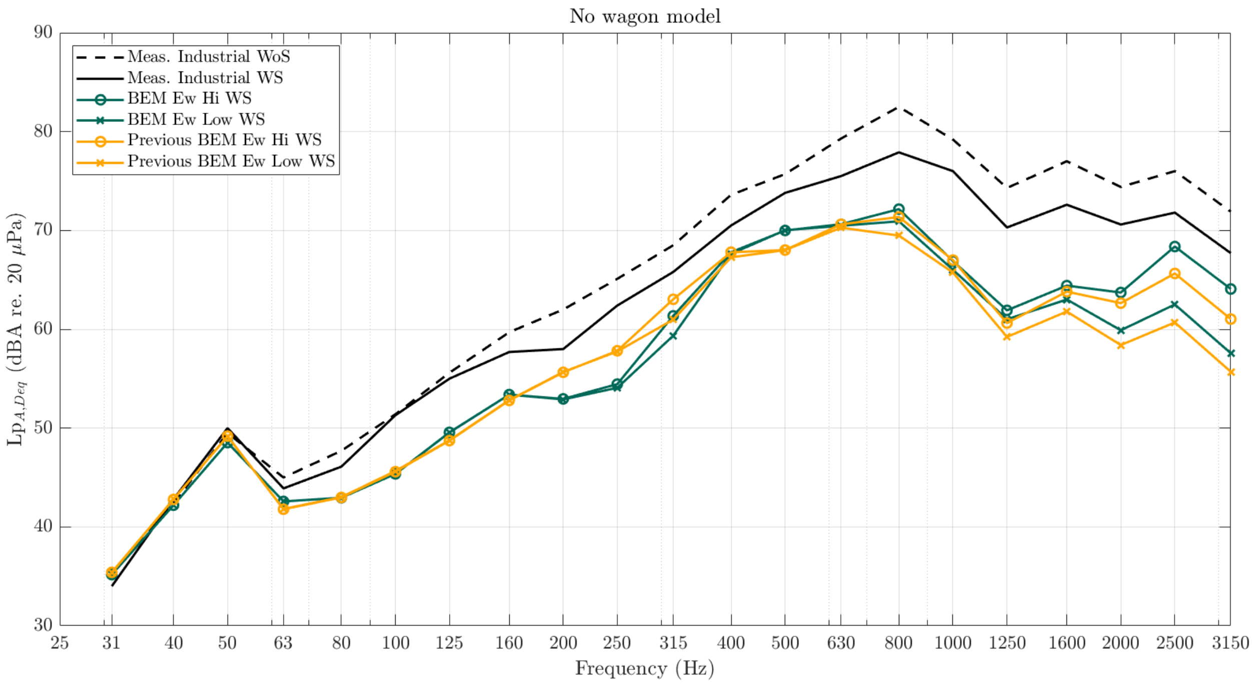

Figure 4.22: *Sound pressure level results from the Quiet City model configuration (calculated from the industrial train measurement).*

4.2.3.2 Nya Östra skolan

LHNS - adjacent track (North)

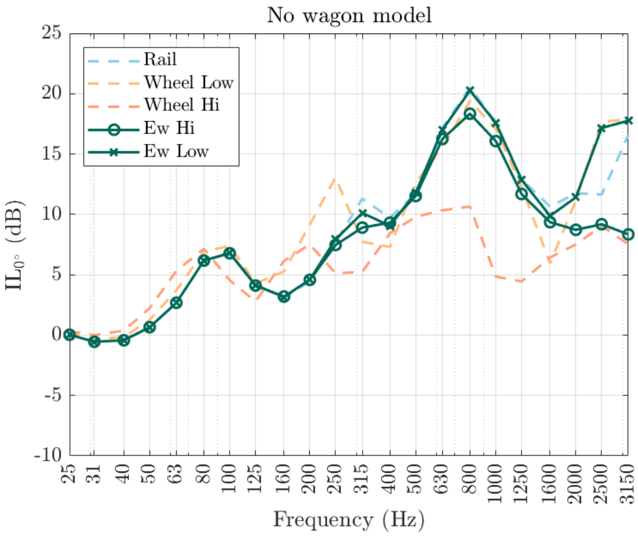

All current BEM results.

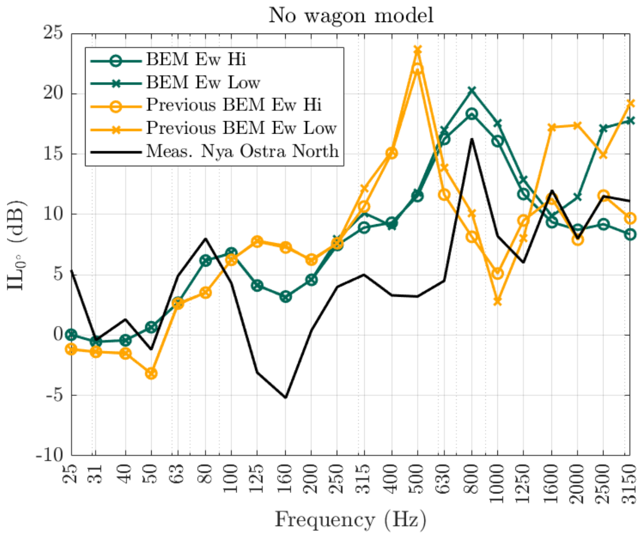

Current and previous Ew BEM results compared to measurement.

Figure 4.23: *IL results from the Nya Östra Skolan (North) model configuration.*

In figure 4.23 note the generally closer alignment with measurement IL trends in the current BEM model compared to previous results.

Figure 4.24: *Sound pressure level results from the Nya Östra Skolan (North) model configuration.*

LHNS - nonadjacent track (South)

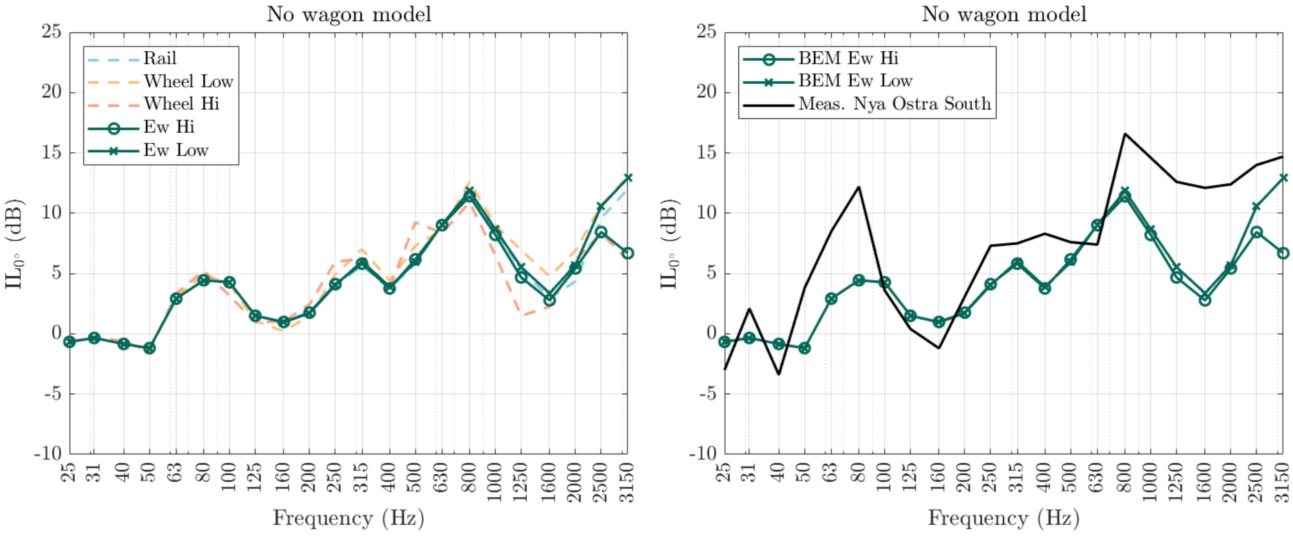

All current BEM results. *Current Ew BEM results compared to measurement.*

Figure 4.25: *IL results from the Nya Östra Skolan (South) model configuration.*

In figure 4.25 note the relatively similar results from all source positions.

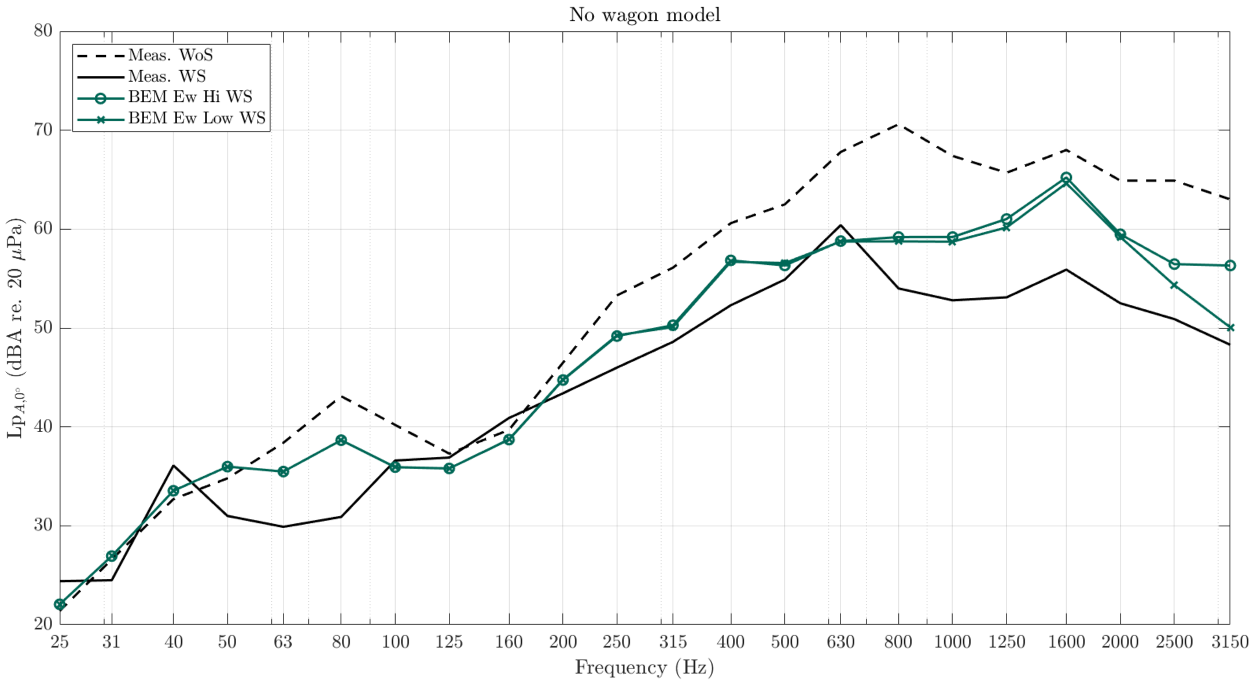

Figure 4.26: *Sound pressure level results from the Nya Östra Skolan (South) model configuration.*

4.2.3.3 Saltsjöbanan

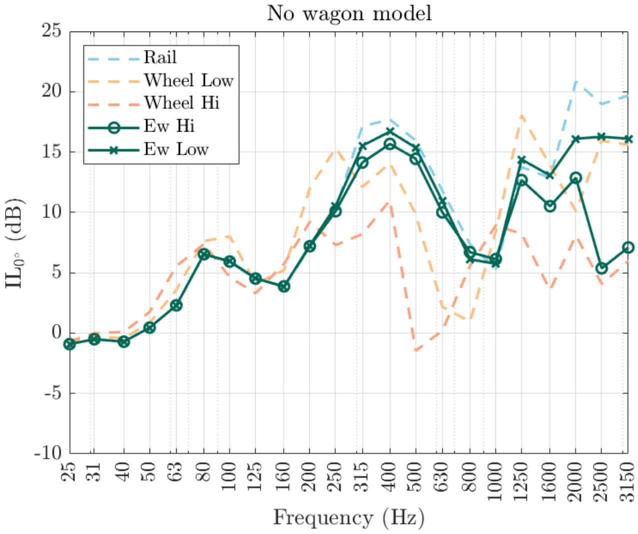

All current BEM results.

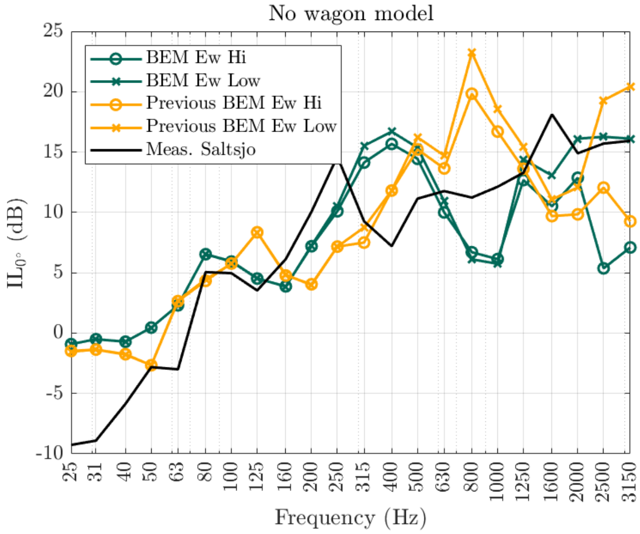

Current and previous Ew BEM results compared to measurement.

Figure 4.27: *IL results from the Saltsjöbanan model configuration.*

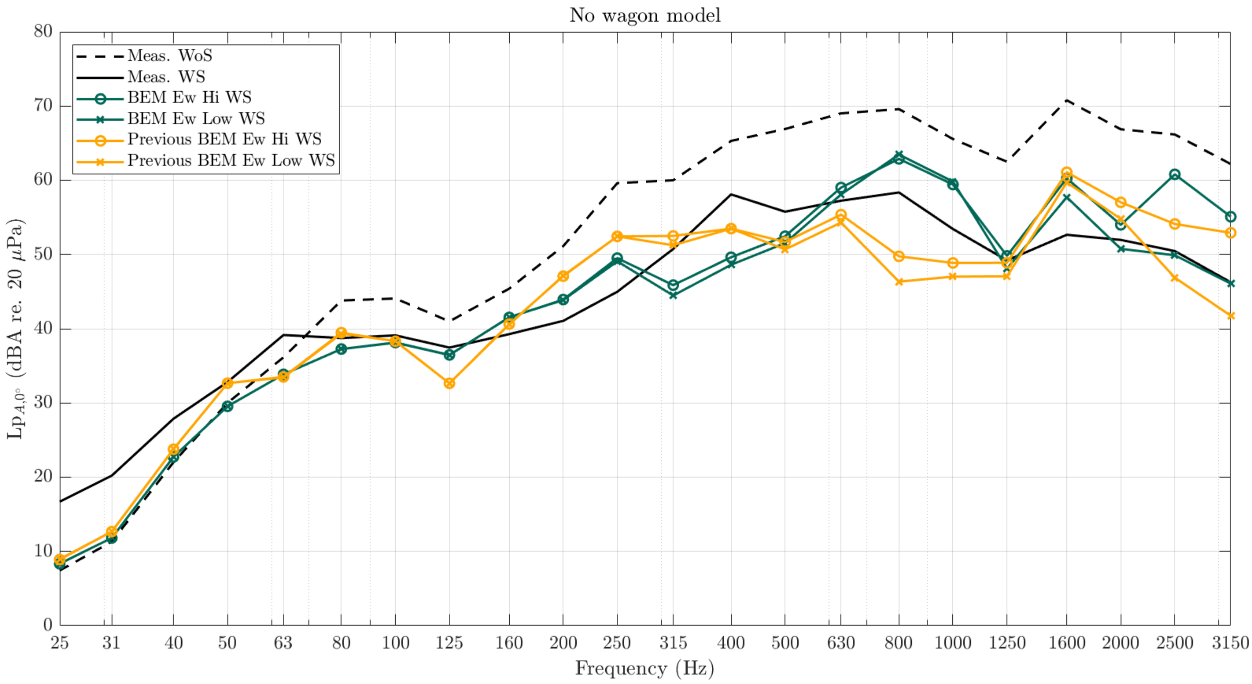

Figure 4.28: *Sound pressure level results from the Saltsjöbanan model configuration.*

4.2.4 Total A-weighted IL comparison

This section presents and compares the total, single value, A-weighted IL results from the BEM simulations and compare them with corresponding values from measurements. First, results from previous and current BEM model simulations that have a comparable measurement are compared in figure 4.29 and 4.30. Results from all simulations are then presented in table 4.2 and discussed. Note that the method used for calculating total A-weighted IL (see section 3.2.3) in this thesis differs from the method used in [1]. Because of this, total A-weighted IL results from the previous BEM iteration have been recalculated using the method as described in 3.2.3.

Passenger train

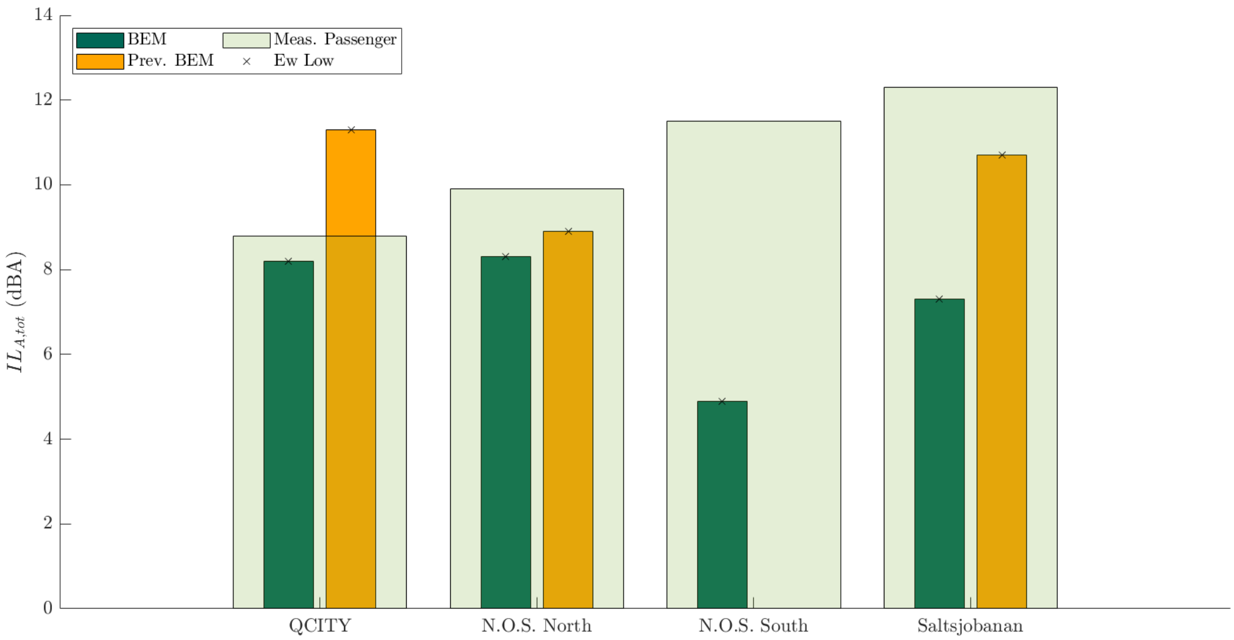

Figure 4.29: *Passenger train total A-weighted IL comparison.*

In figure 4.29 it can be observed that there are large differences in how accurate simulated results are to measured results from measurement to measurement. It can also be noted that the current BEM iteration generally calculates the total IL as being lower than the previous iteration, which is an advantage when comparing with measurements from Quiet City, but a disadvantage when comparing with measurements from Nya Östra Skolan and Saltsjöbanan.

When observing the IL and sound pressure level spectra in section 4.2.1 it can be argued that materially lower total IL in BEM simulations compared to measurements, as seen in Nya Östra Skolan and Saltsjöbanan, are caused by significant frequency-dependent IL deviations in one or two frequency bands. Particularly in the 800 Hz and 1600 Hz frequency bands. In all of these occurrences the wheel source can be seen as providing a more accurate depiction of IL than the rail source, which could potentially indicate that the source energy weighting is not entirely accurate.

Industrial train

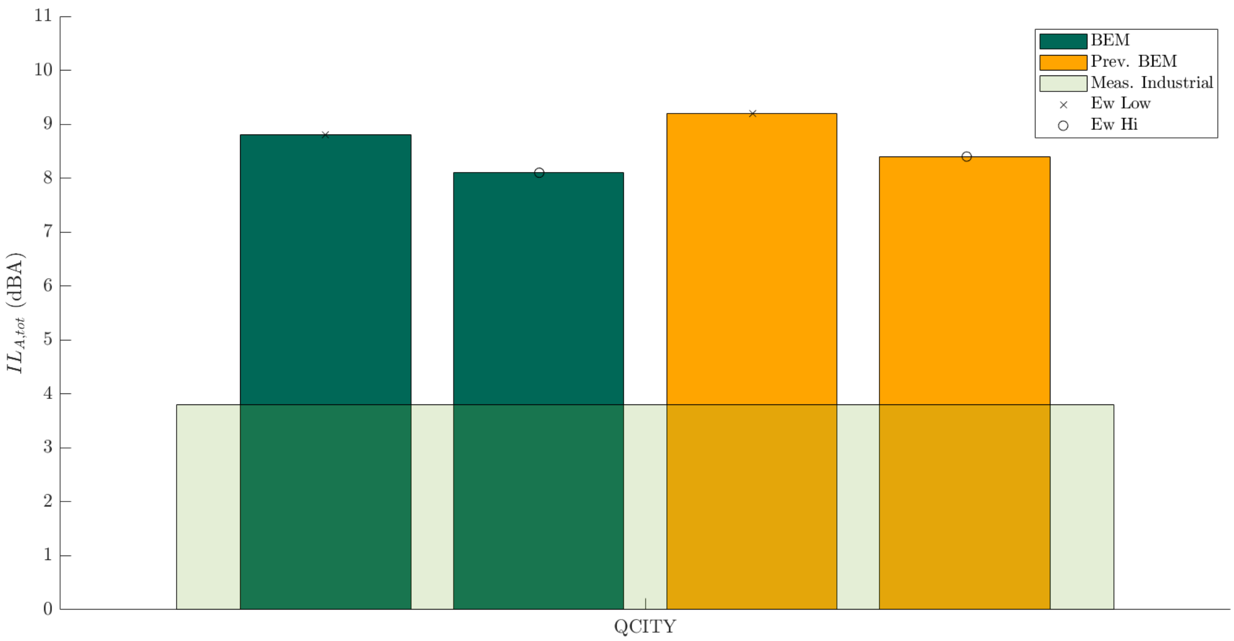

Figure 4.30: *Industrial train total A-weighted IL comparison.*

In figure 4.30 large deviations between measured and simulated total IL results can be observed. When looking in the QCITY chapter of section 4.2.2 it can be seen that IL results are overestimated across more or less the entire frequency range, indicating that the BEM model is not fit for estimating IL for this type of train in the current or previous iteration.

One potential cause could be different source locations in the industrial train, as it can be seen in figure 4.12 that the wheel hi source provides an IL result closer to measured results in frequency bands above 200 Hz. This implies that higher placed sources locations than the ones used in the BEM simulations could be influencing the measurement results. However, with only one set of measurement data for this train type is hard to draw definite conclusions.

All results

Total IL results for all measurements and simulations are found in table 4.2. When comparing the total A-weighted IL results, one main thing is worth noting: Compared to the previous BEM model, the current BEM model predicts slightly lower IL in general (excluding Nya Östra Skolan). This indicates that impedance model used in this thesis provides slightly lower sound absorption than in the previous thesis.

Table 4.2: *Single value A-weighted IL results for all measurements, as well as current and previous BEM simulations.*

$IL_{A,tot}$ (dBA)	Quiet City*	N.Ö.S, North	N.Ö.S, South	Saltsjöbanan
Measured, passenger	8.8	9.9	11.5	12.3
Measured, industrial	3.8	-	-	-
X60 BEM:				
Ew_{low}	8.2	8.3	4.9	7.3
Previous Ew_{low}	11.3	8.9	-	10.7
Industrial wagon BEM:				
Ew_{hi}	8.1	8.6	6.2	6.8
Ew_{low}	8.8	9.7	7	7.8
Previous Ew_{hi}	8.4	6	-	10.5
Previous Ew_{low}	9.2	7	-	10.5
No wagon BEM:				
Ew_{hi}	9.4 / 9.4 **	12	6.5	9
Ew_{low}	10.4 / 10.5 **	14	7.2	10.3
Previous Ew_{hi}	9.9 / 10.1 **	8.7	-	11.8
Previous Ew_{low}	11.1 / 11.4 **	9.8	-	13.6

* data value is calculated from a third octave frequency band interval of 31.5 Hz - 3150 Hz.
All other results are calculated from a third octave band interval of 25 Hz - 3150 Hz.
** X60 result / industrial wagon result.

4.3 Recommended future improvements

The results yielded from the updated impedance model which has been the focus of this thesis show potential, especially regarding the frequency-dependent IL trends for passenger trains. Generally it can be argued that these results show a closer fit with comparable measurement data when compared to previous BEM model implementation. However, a few specific frequency bands deviated significantly from measured results. As such, certain aspects of the calculation model need further examination in order to fulfill the goal of a implementable tool in STA projects. The main improvement areas can be listed as the following:

- Source locations and relative energy distribution
- Additional validation data

Each of these points will be described in further detail below.

Source locations and relative energy distribution

Due to the low height of LHNS, source location on the train is an important factor in determining the potential attenuation that the screen can provide. Additionally if the train has multiple sources it is important to know the relative energy distribution between the sources. From a general overview of the results in chapter 4.2 it can be deduced that the default source locations from the Nord2000 rail model with an assumed relative energy distribution of an X2000 train, discussed in chapter 2.2.2, work reasonably well in case of passenger trains. However, as can be seen in the QCITY chapter of section 4.2.2, this is not true for different types of trains. In order to make the calculation model more generally applicable, this topic needs to be further investigated.

Additional validation data

In order to continue developing the BEM model in any meaningful way, more validation data for checking the validity of simulated LHNS results needs to be acquired. For this thesis and the previous thesis, 3 measurement reports with greatly differing measurement procedures have been used. In the case of industrial trains only one measurement is available. More data is needed in order to make informed decisions regarding what can be considered a quirk of the validation data, and what can be considered a quirk of the calculation model. This is particularly relevant in finding the cause of the discrepancies in the 800 Hz and 1600 Hz frequency bands of certain simulated results.

5

Conclusion

The goal of this thesis has been to improve the boundary element method (**BEM**) model implemented in the thesis written by P. Eriksson, for use in railway applications. To achieve this an investigation into the surface impedance of train tracks has been performed, using results from impedance measurements performed at train tracks as validation data for impedance parameter determination. Based on findings from conducted measurements, it is found that using the slit-pore impedance model, the following impedance parameters are most representative of measured train tracks:

Material:	d (m)	σ (Ns/m^4)	ϕ (%)
Train tracks	0.45	1000	49.1

Implementation of the determined impedance parameters in BEM simulations shows a general improvement in frequency-dependent insertion loss (**IL**) trends, relative to existing measured results, when compared with previous results. However, in some cases specific frequency bands deviate significantly from measurements. This greatly influences the calculation of total IL results. Additionally, it is found that the current implementation of the train source model is not suitable for non-passenger trains.

In the thesis, BEM-simulated low-height noise screen (**LHNS**) results have been compared with a limited set of measurements from other projects. This has been somewhat adequate for analysing the effectiveness of the updated impedance model, since a separate validation process was made for this purpose. If a continuation of this work is to be made, focusing on more train-specific aspects such as source strength and distribution, more validation data is necessary.

The limited set of validation data for train-LHNS setups makes drawing definitive conclusions about the effectiveness of the developed calculation model hard to do. However, it can be argued that if the highlighted improvement possibilities are addressed, there is potential that the developed BEM-model can become adequate for use in the planning stage of infrastructure projects.

Bibliography

[1] P. Eriksson, "Investigation of prediction methods for low height noise barrier implementation," master's Thesis, Chalmers University of Technology, 2022.

[2] B. v. d. Aa, *Road traffic noise reduction by multiple scattering and absorption mechanisms.* PhD thesis, Chalmers University of Technology, 2015. ISBN: 9789175972114.

[3] M. Kleiner, *Acoustics and Audio Technology.* Sept. 2011.

[4] A. S. Dukhin and P. J. Goetz, "Fundamentals of Acoustics in Homogeneous Liquids," in *Studies in Interface Science*, vol. 24, pp. 91–125, Elsevier, 2010.

[5] K. Attenborough, S. I. Hayek, and J. M. Lawther, "Propagation of sound above a porous half-space," *The Journal of the Acoustical Society of America*, vol. 68, pp. 1493–1501, Nov. 1980.

[6] C. Rubio, S. Castiñeira-Ibáñez, J. V. Sánchez-Pérez, P. Candelas, F. Belmar, and A. Uris, "Open Acoustic Barriers: A New Attenuation Mechanism," in *Advances in Noise Analysis, Mitigation and Control*, IntechOpen, Oct. 2016.

[7] M. Delany and E. Bazley, "Acoustical properties of fibrous absorbent materials," *Applied Acoustics*, vol. 3, pp. 105–116, Apr. 1970.

[8] K. Attenborough, I. Bashir, and S. Taherzadeh, "Outdoor ground impedance models," *The Journal of the Acoustical Society of America*, vol. 129, pp. 2806–19, May 2011.

[9] "Zbloc norden ab." https://sbloc.se/bullerskarm/privatperson/. [Online].

[10] H. G. Jonasson and S. Storeheier, "Nord 2000. New Nordic Prediction Method for Rail Traffic Noise,"

[11] X. Zhang, "Prediction of high-speed train noise on Swedish tracks,"

[12] X. Zhang, "Tuning of the acoustic source model : Aiming at accurate noise assessments along high-speed railways," tech. rep., 2015.

[13] NORDTEST, "Ground surfaces: Determination of the acoustic impedance (NT ACOU 104)," Nov. 1999.

[14] J. Nielsen, O. Lundberg, and N. Renard, "Quiet City Transport," 2005.

[15] P. Ragnarsson, "Nya Östra Gymnasiet - Ljudnivåer från tågtrafik före och efter montage av spårnära skärmar," 2023.

[16] NORDTEST, "Railway traffic: Noise (NT ACOU 098)," May 1997.

[17] V. Wetterblad, "RAPPORT 589476-A, Saltsjöbanan," Dec. 2013.

[18] B. v. d. Aa and J. Forssén, "Time-domain simulations of low-height porous noise barriers with periodically spaced scattering inclusions," 2014.

DEPARTMENT OF ARCHITECTURE AND CIVIL ENGINEERING
DIVISION OF APPLIED ACOUSTICS
CHALMERS UNIVERSITY OF TECHNOLOGY
Gothenburg, Sweden 2024
www.chalmers.se